Science of Remote Sensing 5 (2022) 100050

Contents lists available at ScienceDirect

Science of Remote Sensing

journal homepage: www.sciencedirect.com/journal/science-of-remote-sensing

Direct and automatic measurements of stem curve and volume using a high-resolution airborne laser scanning system

Eric Hyyppä [a,*], Antero Kukko [a,b], Harri Kaartinen [a,c], Xiaowei Yu [a], Jesse Muhojoki [a], Teemu Hakala [a], Juha Hyyppä [a,b]

[a] Department of Remote Sensing and Photogrammetry, Finnish Geospatial Research Institute, 02150, Espoo, Finland
[b] Department of Built Environment, Aalto University, School of Engineering, P.O. Box 11000, FI-00076, Aalto, Finland
[c] Department of Geography and Geology, University of Turku, FI-20014, Turku, Finland

ARTICLE INFO

Keywords:
Airborne laser scanning
Mobile laser scanning
Handheld laser scanning
Individual tree detection
Stem curve

ABSTRACT

Today, high-quality reference tree measurements, including the position, diameter, height and volume, are cumbersome and slow to carry out, but highly needed for forest inventories based on airborne laser scanning. Mobile laser scanning technologies hold the promise for collecting reference data for forest inventories with an extremely high efficiency. Perhaps, the most efficient approach for reference data collection would be to mount a high-resolution laser scanning system on board an airborne vehicle flying at a low altitude above the forest canopy since this would allow recording reference samples of individual trees with the speed of flight. To demonstrate the potential of this technology, we mounted an in-house developed HeliALS-DW laser scanning system on board a helicopter and collected point cloud data in a boreal forest on three test sites containing a total of 1469 trees. The obtained point clouds incorporated sufficiently many high-quality stem hits for estimating the stem curves and stem volumes of individual trees since the point clouds had a relatively high point density of 2200–3800 echoes/m^2, and the scanner had been tilted by 15° from the nadir to increase the possibility of recording stem hits. To automatically estimate the diameters at breast height (DBH) and stem curves of individual trees, we used algorithms designed to tolerate moderate drifts in the trajectory of the laser scanner. Furthermore, the stem volumes of individual trees were computed by using the estimated stem curves and tree heights without any allometric models. Using the proposed methods, we were able to estimate the stem curves with a root-mean-square error (RMSE) of 1.7–2.6 cm (6–9%) while detecting 42–71% of the trees. The RMSE of stem volume estimates was 0.1–0.15 m^3 (12–21%). We also showed that the tree detection rate could be improved up to 87–96% for trees with a DBH exceeding 20 cm if slightly larger average errors for the stem attributes were allowed. Our results pave the way for using high-resolution airborne laser scanning for field reference data collection by conducting direct measurements of tree stems with a high efficiency.

1. Introduction

Forest provides economical, ecological and social benefits to humans, such as timber, biofuel, climate regulation, water supply and regulation, air purification, erosion control, habitat for biodiversity, and many other ecosystem services. As an example, the EU's forest sector accounts for 10% of global annual carbon sinks (EU commission, 2021) and forest is home to more than 80% of the terrestrial biodiversity within the EU region (IUCN, 2021). Furthermore, the EU's forest sector employs 22 million people and accounts for an annual turnover of 2 trillion euros in bioeconomy (Future of the European Forest-Based Sector, 2018). These ecosystem services are, unfortunately, competing and even conflicting with each other. For example, the abundance of dead wood is considered to be an indicator of forest biodiversity, since many threatened species are dependent on decaying wood as a habitat. However, dead wood is also a slow carbon source. Thus, there is an urgent need for tools to optimize the forest value chain on a societal level.

Forest data is typically collected with forest inventories, the objective of which is to provide the fundamental information for all decision-

* Corresponding author.
E-mail addresses: eric.hyyppa@nls.fi (E. Hyyppä), antero.kukko@nls.fi (A. Kukko), harri.kaartinen@nls.fi (H. Kaartinen), xiaowei.yu@nls.fi (X. Yu), jesse.muhojoki@nls.fi (J. Muhojoki), teemu.hakala@nls.fi (T. Hakala), juha.hyyppa@nls.fi (J. Hyyppä).

https://doi.org/10.1016/j.srs.2022.100050
Received 17 January 2022; Received in revised form 4 April 2022; Accepted 5 April 2022
Available online 9 April 2022
2666-0172/© 2022 The Authors. Published by Elsevier B.V. This is an open access article under the CC BY-NC-ND license (http://creativecommons.org/licenses/by-nc-nd/4.0/).

making concerning forest industry and uses of forests relevant to human interventions, such as harvest planning and natural conservation. In the Nordic countries, forest inventory is performed at the national scale with the help of airborne laser scanning (ALS) measurements providing the knowledge of average forest resources both at the country, regional, and stand levels (Næsset et al., 2004; Kangas et al., 2018). The stand level information incorporates mean or sum values of the main forest attributes for, e.g., 16-m-by-16-m-size raster cells. This area-based prediction provides adequate data for most of the decision making, but there is also a clear trend indicating that individual tree maps are needed in the future. If properly calibrated, such maps can contribute to multiple benefits that may include, for example, more accurate forest inventory data, improved digital and electronic wood trade, assistance in certification of wood origin, improved estimation of the value of forest, and assistance of forest harvesters in their localization and information support. The possibility of constructing large-scale individual tree maps is currently mainly limited by the lack of accurate field reference data at the individual tree level, whereas methods for estimating attributes of individual trees from ALS data have been known since 1999 (Hyyppä and Inkinen, 1999; Wang et al., 2016; Zhen et al., 2016). Reference data containing information of, e.g., stem diameters, stem volumes and tree heights of individual trees would be required for calibrating the models designed for estimating individual tree attributes from the nation-wide ALS data.

There are several technologies to provide field reference data of individual trees, such as pseudolite technology using triangulation combined with manual measurements, data collected with a harvester head during the chopping of wood, smartphone-based crowdsourcing (Tomaštík et al., 2017), terrestrial laser scanning (TLS) (Simonse et al., 2003; Bienert et al., 2007; Raumonen et al., 2013; Liang et al., 2016), personal laser scanning (Chen et al., 2019; Balenović et al., 2021) and mobile laser scanning (MLS) (Hyyppä et al., 2020a) mounted on board a harvester (Miettinen et al., 2010), an all-terrain vehicle (ATV) (Liang et al., 2014a), a backpack (Oveland et al., 2018), or an unmanned aircraft vehicle (UAV) (Wallace et al., 2012; Hyyppä et al., 2020b). Especially TLS has been studied extensively during the past decade thanks to the high-quality point clouds that can be collected with the TLS system. As a downside of TLS, it takes a long time to collect location-aware reference data for a large number of trees. Mobile laser scanning technologies hold the promise of collecting reference data with one or multiple orders of magnitude higher speeds than is possible with TLS. Most likely, the fastest approach for reference data collection would be to mount a laser scanner on board a UAV or a helicopter flying relatively low above the forest canopy. With such an approach, it would be feasible to measure up to tens of thousands or even hundreds of thousands of reference trees within a single day.

In addition to the swiftness of data collection, the accuracy of the field reference data is crucial. In the following, we focus on stem volume estimation since the stem volume is not only one of the most important tree attributes, but it is also rather difficult to estimate accurately with currently available technologies. In boreal forest conditions, TLS has been shown to enable stem volume estimation with a relative root-mean-square error (RMSE) of approximately 10% (Liang et al., 2014b) provided that the tree tops are not occluded in the data. Recently, Shimizu et al. (2022) showed that a combination of TLS data and UAV laser scanning (UAVLS) data improves the RMSE of stem volume estimation down to 10% even though the forest canopy would be occluded in the TLS data. In the field of MLS, the first studies providing stem volume estimates of individual trees reported relative RMSE ranging approximately from 20% to 50% in easy and medium difficult boreal forest conditions (Liang et al., 2018, Liang et al., 2019; Bienert et al., 2018). Importantly, such a large average error is not satisfactory for operational field reference data collection, for which a relative RMSE of approximately 10% would be required. Recently, we have shown that the stem volume of individual pine and birch trees can be estimated with a relative RMSE of approximately 10% from 3D data collected with a multitude of MLS systems, including backpack, handheld and under-canopy UAV systems (Hyyppä et al., 2020a; Hyyppä et al., 2020b; Hyyppä et al., 2020c; Hyyppä et al., 2021b). The key improvements enabling such a low average error included the use of stem curve information to compute the stem volume estimates and the development of point cloud processing algorithms that were robust against moderate positional drifts in the estimated trajectory of the mobile laser scanner.

To the best of our knowledge, there has been only one previous study on deriving stem curves of individual trees from point clouds collected by airborne platforms even though this was proposed by Jaakkola et al. already in 2017 (Jaakkola et al., 2017). In 2019, Liang et al. (2019) concluded that the errors of stem curves estimated from UAVLS data were far higher than those obtained from TLS or MLS data, or even those obtained with conventional individual-tree-based estimation (Hyyppä and Inkinen, 1999). A slightly higher number of studies have investigated the feasibility of measuring the diameter at breast height (DBH) directly from dense UAVLS point clouds (Jaakkola et al., 2017; Brede et al., 2017; Kuželka et al., 2020; Wieser et al., 2017; Vandendaele et al., 2021). Here, direct diameter measurements mean that the stem diameter was obtained by fitting a circle or a cylinder to the point cloud data, whereas the conventional approach is to predict the DBH from the tree height and other canopy-related tree attributes extracted from the ALS data (Hyyppä and Inkinen, 1999; Yu et al., 2011; Hao et al., 2021). Puliti et al. (2020) utilized UAVLS point cloud data to conduct semi-manual DBH measurements on a small subset of the trees to train a random forest model for predicting the DBH of the remaining trees from crown attributes estimated from the same UAVLS data. The predicted DBH values and estimated tree species information were further used to compute the total stem volume at the plot, stand, and forest levels.

In this paper, we show for the first time that the stem curves of individual trees can be estimated with a high accuracy by using direct and automatic measurements from relatively dense (2200–3800 pt/m^2) point clouds collected with an airborne laser scanner mounted on a helicopter. Our work can be viewed as an extension to our previous studies, in which we have assessed the accuracy of direct stem curve measurements from point cloud data collected by an under-canopy flying UAV (Hyyppä et al., 2020a; Hyyppä et al., 2020b). As compared with the under-canopy measurements, more expensive sensors were required in this study for obtaining high-quality measurements of the stems. Namely, the point spacing and beam size must be sufficiently small to enable direct measurements of the stems, but both of these properties deteriorate as a function of the range due to laser beam divergence and insufficient point spacing. The direct stem curve measurements from an above-canopy platform are advantageous since the point cloud is already georeferenced thanks to a strong Global Navigation Satellite System (GNSS) signal and other characteristics of the tree crowns can be easily derived from the same data. Importantly, the proposed approach also enables the collection of reference data with a rate that is up to several hundred times faster than what can be achieved with multiscan TLS measurements. As pointed out in Puliti et al. (2020), it is not necessary to estimate the stem curve for all of the trees at a given test site to use the results as a field reference data set. Thus, we have designed our algorithms to detect only such trees, for which the stem curve can be estimated with a low RMSE of 5–10%. In this paper, we analyze the completeness rate of stem detection and errors of stem curves, DBHs and stem volumes estimated for such reference trees. The accuracy of tree height measurements from ALS data has already been studied before (see e.g., Hyyppä and Inkinen (1999), Wallace et al. (2014), Jaakkola et al. (2010), and Wang et al. (2019)), and, therefore, we do not investigate this matter in the current study.

2. Material and methods

2.1. Scenarios for stem attribute estimation from ALS data

In this paper, we studied two scenarios for ALS-based stem attribute

estimation. In the first scenario named as *high-quality trees*, we aimed to detect only those trees, for which we could estimate the stem attributes with a high accuracy. These trees are aimed to be used as a training data set for ALS-based forest inventories. Such inventories require a large number of accurately measured reference trees, which are conventionally obtained by manual field measurements. In the second scenario named as *as many trees as possible*, we aimed to detect as many stems as was possible with the cost of increased average errors in the estimated stem attributes. This scenario corresponds to conducting a small-scale forest inventory at the individual tree level for medium-sized and large trees. By finding almost all of the trees, the bias of ALS-based inventories can be reduced. The obtained map of tree locations can also be useful for point cloud registration purposes (Hyyppä et al., 2021a). As explained in Sec. 2.5, the results of the two scenarios can be obtained with the same algorithm but with different parameter values. In Sec. 3.3, further discussion regarding the applications of the two scenarios are provided based on the accuracy of the obtained results.

2.2. Test area

The study was conducted on three test sites that were located in the Southeastern part of Finland in the Lappeenranta region (61°03′ N 28°11’ E). The study area was located in a managed forest in the boreal forest zone, and Norway spruce (*Picea abies*) was the dominant tree species on all of the three test sites. A large majority of the spruces at the test sites were mature, and therefore, the lower parts of their trunks were not severely occluded by branches or needles as can be seen from Fig. 1 that shows photographs of the test sites 1 and 3.

We provide detailed descriptive statistics of the trees located at the test sites in Table 1. Importantly, the statistics are based on stem attributes estimated from point cloud data collected with a handheld ZEB Horizon scanner (GeoSLAM, UK). A handheld laser scanner was selected to provide the field reference data, since we needed high-quality stem curves for a large number of reference trees (See Sec. 2.6 for details). In total, the three test sites of the study covered an area of approximately 2.2 ha and incorporated in total of 1469 trees. The average number of stems per hectare was 690 stems/ha within the study site 1, 470 stems/ha within the site 2, and 1000 stems/ha within the site 3. The stem densities varied significantly within each test site, and, for example, the local stem density within the site 3 varied between 320 stems/ha and 2400 stems/ha.

Table 1
Descriptive statistics of the trees located on the three test sites. The statistics are based on stem attributes estimated from point cloud data collected with the handheld ZEB Horizon laser scanner (see Sec. 2.6). We report the standard deviation for DBH, tree height and stem volume within the parentheses. For stem density, we report the minimum and maximum values within each test site, respectively.

Test site	Number of trees	Area (ha)	Stem density (1/ha)	Mean DBH (cm)	Mean tree height (m)	Mean stem volume (m^3)
1	421	0.6	690 [130, 1400]	24.8 (±7.3)	21.1 (±4.3)	0.64 (±0.39)
2	423	0.9	470 [65, 970]	28.5 (±6.1)	22.1 (±3.8)	0.89 (±0.36)
3	625	0.7	1000 [320, 2400]	21.9 (±6.2)	18.2 (±4.1)	0.44 (±0.29)

Table 2
Technical specifications of the airborne laser scanning system used for this study.

Property	Value
Scanner	Riegl VUX-1HA
Altitude AGL (m)	80
Flight speed (m/s)	9.5
Beam divergence (mrad)	0.5
Beam footprint (cm)	4
Pulse rate (kHz)	1017
Scan line rate (Hz)	200
Point spacing (cm)	9.8
Separation of scan lines (cm)	4.8
Resulting point density (echoes/m^2)	2200 – 3800

2.3. Acquisition of dense airborne laser scanning point clouds

To collect dense airborne laser scanning point clouds of the forests on the three test sites, we used a FGI-developed laser scanner system known as HeliALS-DW that was mounted on a helicopter. A similar system could be mounted on a UAV as well. Relevant qualities of the laser scanner system have been summarized in Table 2. The HeliALS-DW system incorporated a Riegl VUX-1HA scanner (Riegl GmbH, Austria) and a GNSS-IMU positioning system based on a LITEF UIMU-LCI inertial measurement unit (IMU), a NovAtel Flexpak6 GNSS receiver and GGG-703 antenna. The ALS measurements were conducted individually for each test site in October 2020. For each test site, the flight trajectory of the helicopter was planned to consist of multiple perpendicular flight lines forming a 2D rectangular grid with a flight line separation of 50 m. The flight speed of the helicopter was 9.5 m/s, whereas the flight altitude was approximately 80 m above the ground level corresponding to 50–60 m above the forest canopy. See Fig. 2(a) and (b) for a schematic illustration of the measurement principle.

The VUX-1HA laser scanner used in the study had a pulse rate of 1017 kHz and it provided 200 scan lines per second. These qualities resulted in an angular resolution of 1.2 mrad corresponding to a point spacing of 98 mm at a range of 80 m. Based on the average flight velocity of the helicopter, the spacing between consecutive scan lines was 48 mm. Importantly, the scan planes were intentionally tilted 15° forward with respect to the vertical direction in order to increase the possibility to record stem hits as illustrated in the schematic of Fig. 2(a).

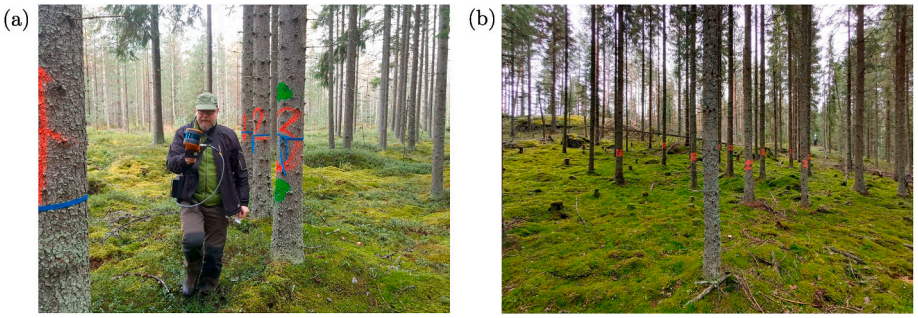

Fig. 1. Photographs taken within (a) the test site 1 and (b) the test site 3. Both of the illustrated test sites were covered by a spruce forest.

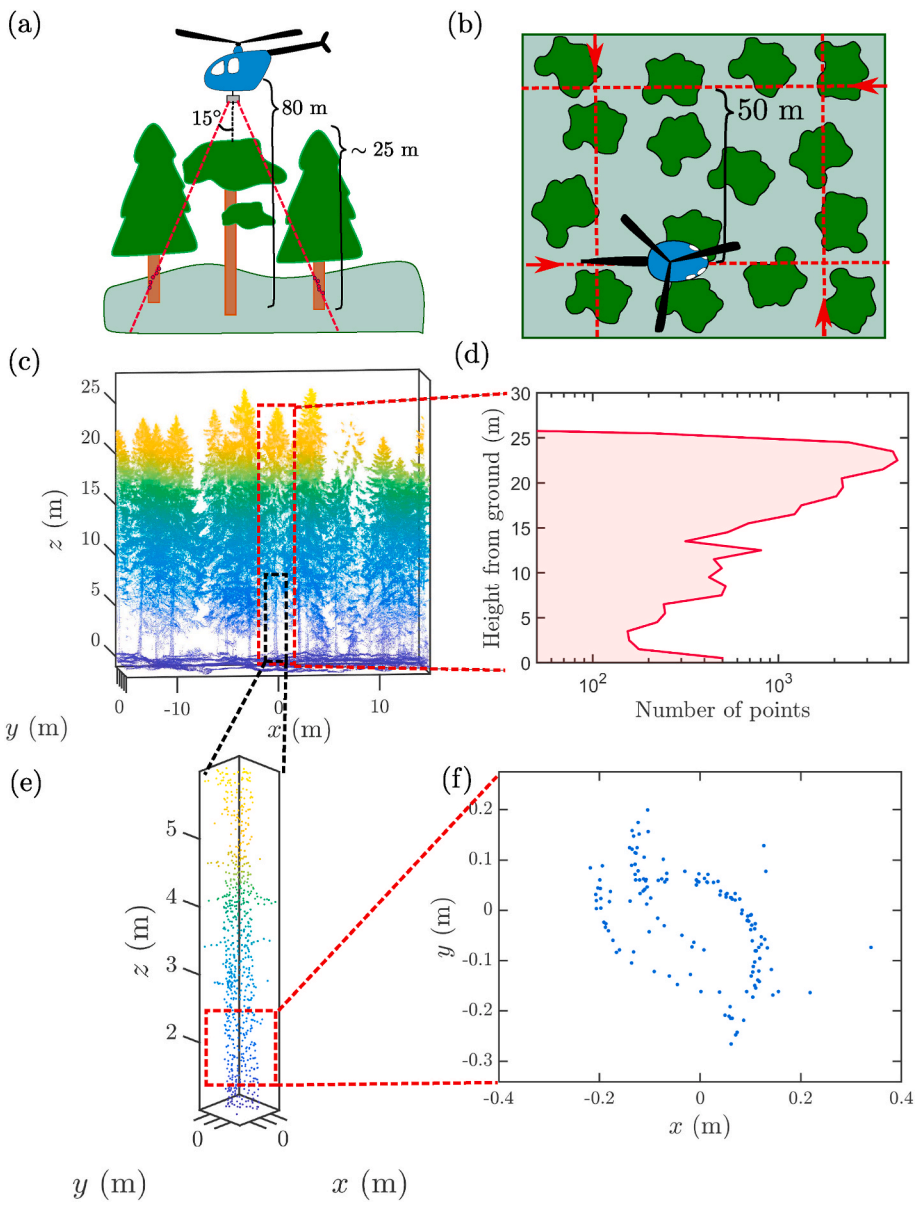

Fig. 2. Schematic illustration of the measurement principle and the resulting point cloud data. (a) The point cloud data was collected using a Riegl VUX-1HA scanner mounted on a helicopter flying 80 m above the ground level. The laser scanner was tilted 15° forward with respect to the vertical direction for improved stem sampling. (b) The test sites were covered using flight lines that formed a square grid pattern. (c) The resulting point cloud after the pre-processing steps from a small region within the first test site. (d) Point count as a function of the height from the ground level for an example tree. The point count was computed using 1-m height intervals by considering points located within a distance of 1 m from the example tree. (e) A close-up to the stem of the example tree. (f) Cross section of the stem in panel (e) in the height interval $z \in [1.5, 2.5]$ m above the ground level. Note the remaining distortion in the pre-processed point cloud that is due to combining data from several flight lines.

2.4. *Pre-processing of dense point clouds*

Several pre-processing steps were required to transform the raw HeliALS-DW data into a point cloud in the global coordinate system. First, we estimated the trajectory of the scanner during the measurements using Waypoint Inertial Explorer (version 8.90, NovAtel Inc., Canada) and nine virtual GNSS base stations from Trimnet service (RINEX 2.11). The GNSS base stations were situated at each of the test sites and at the airfields, where the helicopter took off and landed. Thus, the base stations were located over a region with a radius of 40 km. The differential GNSS solution was obtained by using GPS and GLONASS constellation satellites, and multi-pass tightly coupled computing with a satellite elevation threshold of 12°. During the measurements, the mean number of observed satellites was 12.8. The outputted trajectory was estimated to have a planimetric mean error of 6 mm and a mean elevation error of 9 mm. The estimated mean attitude errors were 0.12, 0.12, and 0.36 arcmin. The sampling rate of the output trajectory data was 200 Hz.

Subsequently, we used RiProcess software (version 1.8.8, Riegl GmbH, Austria) and its MTA and RiPrecision utilities to process the raw VUX-1HA lidar data into the point cloud format with the help of the obtained trajectory. Note that the trajectory and the point could geometry were further improved and optimized in the process. As the first step, a scan alignment tool was used to solve for the boresight misalignment between the laser scanner and the IMU. As a result, the residual alignment error corresponding to a 3D standard deviation was estimated to be 66 mm based on 111015 correspondence planes found from the point cloud data. Subsequently, dynamic trajectory drifting was removed from the trajectory with the help of the multi-pass lidar data. As a result of this step, the positioning of the trajectory was improved on average by less than a millimetre in plane and about 7 mm in elevation. The corresponding average attitude corrections were 0.007, 0.007 and 0.002 arcmin for the roll, pitch and heading angles, respectively. After these optimization steps, the residual 3D error (STD) for the whole point cloud data was estimated to be 51 mm based on 195178 automatically detected planar features. The final point cloud product was exported in LAS 1.2 format for further processing. Points with reflectance values lower than −25 dB or higher than 5 dB were removed from the final point cloud. In Figs. 2(c) and Fig. 3, we illustrate the obtained point cloud products after the pre-processing steps.

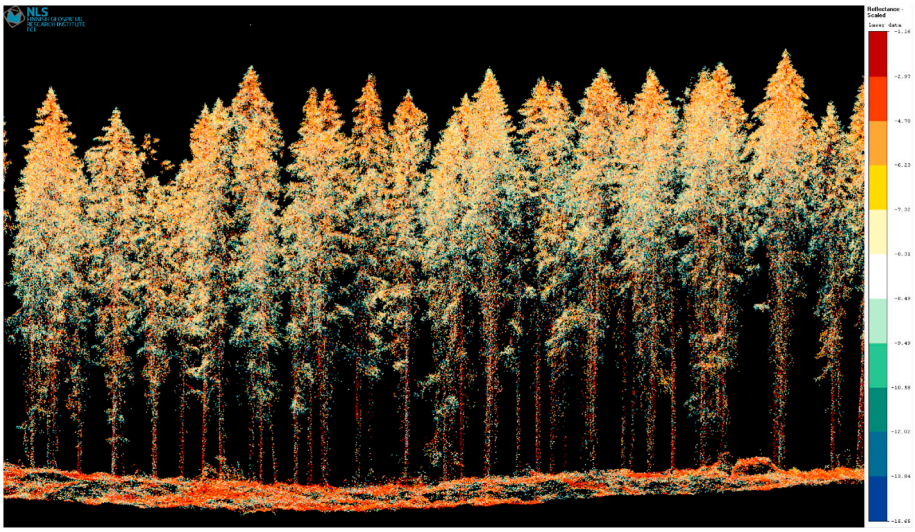

Fig. 3. Cross section of a pre-processed point cloud obtained with the HeliALS-DW system. The colors of each point correspond to reflectance values such that a high value of reflectance is denoted by red color and a low value of reflectance is denoted by green/blue color. (For interpretation of the references to color in this figure legend, the reader is referred to the Web version of this article.)

The point density in the final point cloud, including all laser echoes, was 3800 pt/m^2 within the site 1, 2200 pt/m^2 within the site 2, and 2900 pt/m^2 within the site 3. The minimum point density within any of the test sites was 800 pt/m^2, whereas the maximum point density was 6000 pt/m^2. Importantly, the point clouds contained a sufficiently high number of stem hits enabling direct estimation of stem attributes. In Fig. 2(d), we show the point count within 1-m height intervals as a function of the height from ground for an example tree within the site 1. Even though the majority of the points were reflected from the forest canopy, we see from the figure that the number of stem hits exceeded 100 for each 1-m height interval in the range of $z \in [1.0, 10.0]$; m. As can be seen from Fig. 2(e), the number of stem hits is sufficient for the stems to be clearly visible in the point cloud data, and thus, it is possible to directly estimate many important stem attributes, such as the stem curve, from the ALS point clouds.

2.5. Algorithms for the direct estimation of stem attributes

To obtain direct estimates of the stem curves, DBHs, and stem volumes of individual trees from the ALS point clouds, we used an algorithmic work flow that is fully automatic and illustrated in the flow chart of Fig. 4. As the first step of the work flow, the digital terrain model (DTM) was generated and the point clouds were normalized by subtracting the ground level from the z-coordinates of all the points. Subsequently, watershed segmentation was applied to divide the point clouds into smaller regions with the goal to reduce the running time of the stem detection algorithm. In the next step, the stems of individual trees were detected and their stem curves were estimated using an algorithm closely resembling the method that we have utilized previously to estimate stem curves from point cloud data collected with ground-based mobile laser scanning systems (Hyyppä et al., 2020b; Hyyppä et al., 2020c). Finally, the heights of the detected trees were determined, and the combined information of tree heights and stem curves was used to estimate the stem volume for each detected tree. We used Matlab to implement all the point cloud processing algorithms.

In the following subsections, we provide a more detailed description of the algorithms that were used for the stem attribute estimation. However, we aim to keep the descriptions concise since the algorithms are relatively similar to those that we have utilized in our previous work for stem attribute estimation from point cloud data collected with ground-based MLS systems (Hyyppä et al., 2020b; Hyyppä et al., 2020c). However, we emphasize the key differences that are required to obtain accurate stem attribute estimates from the collected high-resolution ALS point clouds that have a far lower point density than typical point clouds collected with ground-based MLS systems.

2.5.1. Digital terrain model generation and preliminary watershed segmentation

The DTM was determined by utilizing a voxel-based method. In the method, the xy plane was divided into square-shaped pixels with a side length of 2.0 m, and the z axis was partitioned into 25 equispaced height intervals between the minimum and maximum z coordinate within the point cloud. For each xy pixel, the preliminary ground level was evaluated by computing the mean z coordinate of points located within the lowest height interval that contained at least 0.5% of the total number of points within the xy pixel. The final DTM was obtained by filtering the preliminary DTM with a Gaussian kernel having a size of 5-by-5 pixels and a standard deviation of 1.5 pixels in both the x and y directions. After computing the DTM, the z-coordinates of all the points were normalized by subtracting the ground elevation.

To reduce the running time of the stem detection algorithm, we divided the point clouds into smaller regions by applying the watershed segmentation algorithm for the canopy height model (CHM) multiplied by −1. The CHM was estimated by determining the maximum z-coordinate within each xy pixel followed by Gaussian filtering. For the watershed segmentation, we used the watershed-function in Matlab, and therefore the segmentation was based on an algorithm by Meyer (1994), and the seeds were found with a local minimum search. As the final step before stem attribute estimation, we removed all points with the normalized z-coordinate exceeding 30 m since it was known that all the trees at the test sites had a height shorter than 30 m. We attribute the few erroneous points above the height of 30 m to incorrectly resolved ranges caused by, e.g., aerosol scattering, sun light, false detector triggering (e.g. signal ringing) or most probably due to multiple reflections and a failed multiple-time-around (MTA) process.

2.5.2. Stem detection and stem curve measurement

Since the ALS point clouds were obtained by combining data from multiple flight lines, the data suffered from distortions that would have a negative impact on the stem modelling accuracy if not taken properly into account. This is exemplified in Fig. 2(f) that shows the stem cross section of an example tree in the height interval of $z \in [1.5, 2.5]$ m. Importantly, it is possible to mitigate distortion-related inaccuracies in the stem curve estimation by dividing the point cloud data into multiple

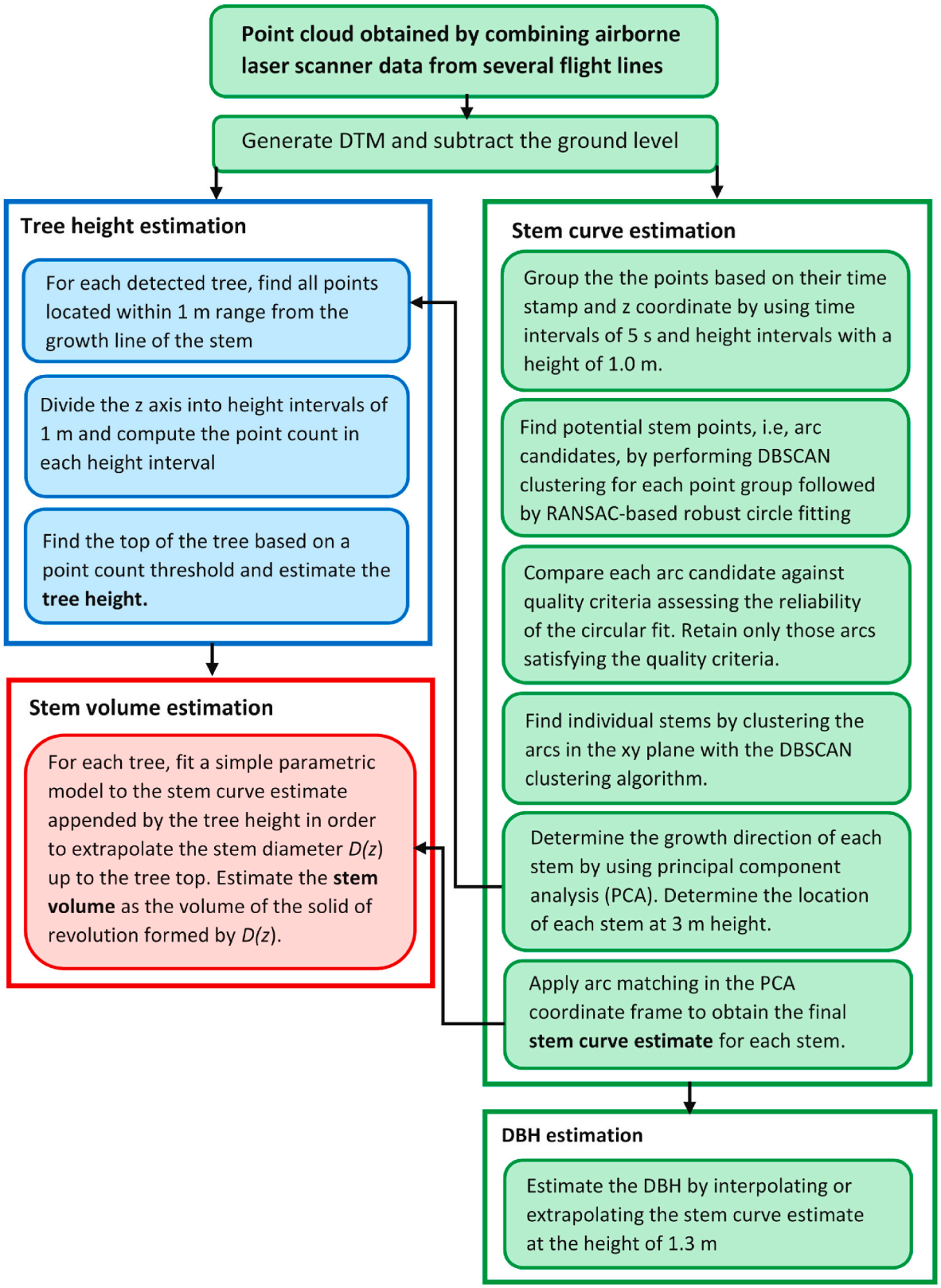

Fig. 4. Flow chart illustrating the algorithms used for estimating stem curves, DBHs, tree heights and stem volumes of individual trees from the collected high-resolution ALS point clouds.

disjoint subsets based on the time stamps of the points as has been done, for example, in Hyyppä et al. (2020b) and Čerňava et al. (2019). This approach is enabled by the fact that the drift in the position and the orientation of the laser scanning system is small during a short period of time, and thus, no distortions are practically present within each subset of the data. Consequently, we applied an arc-based strategy for the stem curve estimation similarly to the approach that we have previously utilized for estimating stem attributes from point clouds collected with ground-based MLS systems (Hyyppä et al., 2020b; Hyyppä et al., 2020c).

The selection of the parameter values for the algorithms was guided based on our previous studies, in which we have utilized the algorithms for the analysis of MLS data (Hyyppä et al., 2020a; Hyyppä et al., 2020b). However, we adjusted the parameter values dependent on the point density to tolerate the relatively low point density of the ALS data. The parameter values were chosen heuristically based on physical properties of the trees, the point cloud, and the scanner instead of optimizing the parameter values by trial and error. Based on our experience, the same set of parameter values works well in different types of forest as long as the same or a similar scanner is used. To obtain the results for the two scenarios introduced in Sec. 2.1, we used different parameter values, which we report as normal text for the scenario *high-quality trees* and within parentheses for the scenario *as many trees as possible*.

To reduce the running time of the stem detection algorithm, we analyzed the point clouds one watershed region at a time. For a given watershed region, we began by dividing the points into a large number of disjoint point groups based on their time stamp and their normalized z-coordinate. To this end, we used time intervals with a duration of 5.0 s and equispaced height intervals with a height of 1.0 m between $z = 0.5$ m and $z = 10$ m. Note that the height of the height intervals was chosen to be a few times higher than in our previous work focusing on ground-based MLS systems (Hyyppä et al., 2020a; Hyyppä et al., 2020b) in order to ensure that each height interval would contain a sufficient number of stem hits.

For each of the obtained point groups, we subsequently aimed to detect arc-like structures using the arc detection method outlined in Hyyppä et al. (2020b). As the first step of the arc detection algorithm, we performed density-based clustering for applications with noise (DBSCAN) (Ester et al., 1996) by utilizing a neighborhood radius of $\varepsilon_1 = 7.5$ cm (7.5 cm) and a minimum point number threshold of $\text{minPts}_1 = 3$ (2) that was chosen to have a low value due to the relatively low point density on stems. Subsequently, we fitted circles to each of the detected clusters with the help of the random sample consensus (RANSAC) framework (Fischler and Bolles, 1981). Importantly, we retained only such clusters, for which more than 75% (75%) of the points were located within a distance of 3 cm (4 cm) from the fitted circular arc. Subsequently, we applied an arc division algorithm (Hyyppä et al., 2020b) with a maximum allowed angular separation of 30°(30°) for each of the retained clusters. Finally, circles were fitted to the remaining clusters using the method described in Al-Sharadqah and Chernov (2009), and the properties of the clusters were compared against the following heuristically chosen quality criteria:

- maximum acceptable standard deviation of the radial residuals: 1.25 cm (1.5 cm)
- lowest acceptable number of points in one arc: 12 (8)
- minimum acceptable stem radius: 5 cm (5 cm)
- maximum acceptable stem radius: 40 cm (40 cm)
- minimum acceptable central angle: 0.6π rad = 108°(0.5π rad = 90°)

The clusters satisfying all the above quality criteria were regarded as stem arcs and used for further processing. Note that the value for the lowest acceptable number of points in an arc was chosen to be approximately one fifth of the value that we have previously used for analyzing data collected with ground-based MLS systems (Hyyppä et al., 2020a).

Subsequently, the centers of the detected arcs were clustered in the xy plane using the DBSCAN algorithm in order to determine, which arcs corresponded to the same stem. To this end, we used a neighborhood radius of $\varepsilon_2 = 25$ cm (25 cm) and a minimum point number threshold of $\text{minPts}_2 = 5$ (2). The neighborhood radius was chosen to be approximately equal to the average DBH of the trees, whereas the minimum point number threshold provided the lower limit for the number of arcs that was required for stem detection. Furthermore, we required that the difference between the z coordinates of the lowest arc and the highest arc needed to exceed 1.0 m (1.0 m) for a cluster to be accepted as a stem. In Fig. 5(a), we illustrate the stem points detected from the point cloud collected on the first test site using the methods described in this section.

To take into account the inclination of the stems, the growth direction for each of the detected stems was estimated using principal component analysis (PCA) applied for the center coordinates of the arcs. For each of the detected stems, the stem diameters were estimated at the heights of $z = j \times 1.0$ m, $j = \{1, 2, \ldots 10\}$, by utilizing the coordinate frame obtained from PCA and the arc matching algorithm proposed in Hyyppä et al. (2020c). We point out that the arc matching algorithm does not perform any global corrections to the point cloud, but it provides a convenient way to visually confirm the success of the stem detection pipeline as illustrated in Fig. 5(b). For each tree, the final stem curve estimate was obtained by filtering out clearly outlying diameter estimates with the help of a simple and automatic outlier detection scheme proposed in Hyyppä et al. (2020c) followed by fitting a cubic smoothing spline (Pollock, 1993; De Boor, 1978) to the remaining diameter estimates. When fitting the smoothing spline, the optimal value for the smoothing parameter was found using leave-1-out cross validation, and each diameter estimate was weighted with the inverse of its 2σ uncertainty estimate.

The final stem curve estimates were further used to predict the DBH of each tree. If the lowest diameter estimate of the tree of interest was located below the height of $z = 1.3$ m, the DBH was obtained by interpolating the cubic smoothing spline at the height of $z = 1.3$ m. If the lowest diameter estimate was located above the height of $z = 1.3$ m, the DBH was obtained by extrapolating the stem curve estimate using either of the following strategies similarly to Hyyppä et al. (2020b):

1. If the height difference between the highest and lowest diameter estimate exceeded 3.0 m, the DBH was predicted by fitting a linear model to the lowest 3 m of the smoothing spline and extrapolating the linear model at the height of $z = 1.3$ m.
2. If the height difference between the highest and lowest diameter estimate was smaller than 3.0 m, the DBH was predicted by fitting a function $D(z) = D_0\sqrt{1 - z/h}$ to the diameter estimates and extrapolating the fitted model at the height of $z = 1.3$ m. Here, h is the estimated tree height and D_0 is the only fitting parameter.

Importantly, our approach for DBH estimation is not only limited to stems, for which the stem is clearly visible around the height of $z = 1.3$ m, but it enables us to estimate the DBH for all the detected stems even though no stem points would be detected at or around the height of $z = 1.3$ m.

2.5.3. Tree height and stem volume measurement

For each of the detected trees, the tree height was estimated using the following procedure: First, we searched for all the points that were located within a distance of 1.0 m from the growth line of the tree obtained from PCA. Subsequently, the z axis was divided into height intervals of height 1.0 m, and the number of points within each height interval was computed. For large trees with a stem diameter exceeding 25 cm, the tree height was obtained as the mean z coordinate of the 5 highest points in the highest height interval bin containing at least 5 points. For small or medium-sized trees having a stem diameter smaller than 25 cm, the tree top was first identified by finding the lowest height interval located above the highest detected arc and containing less than

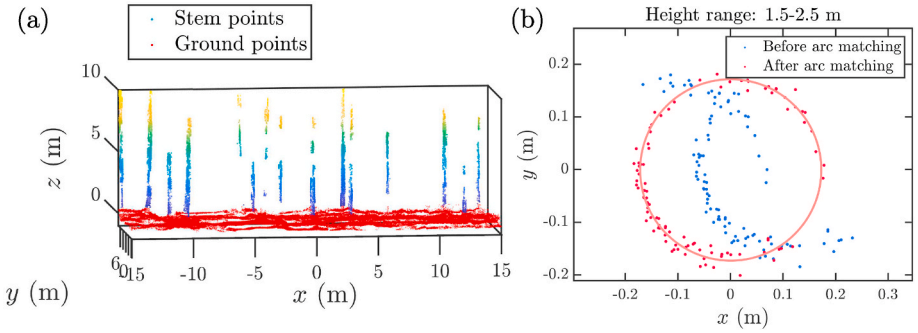

Fig. 5. (a) Stem points and ground points detected from the ALS point cloud collected on the first test site using the stem detection algorithm described in Sec. 2.5.2. (b) Cross section of the stem points for an example tree in the height interval $z \in [1.5, 2.5]$ m before and after applying the arc matching algorithm.

10 points. Subsequently, the tree height was estimated by computing the mean z coordinate of the 5 highest points in a height interval located right below the height interval found in the previous step. Note that trees with small and large diameters were treated using different approaches since trees with a small stem diameter are potentially occluded from the above by neighboring dominant trees.

Finally, the stem volume was calculated for each of the detected trees using the estimated stem curves and tree heights with the help of the method presented in Hyyppä et al. (2020c). To this end, we fitted a parabolic function,

$$D_1(z) = a_2(h-z)^2 + a_1(h-z), \tag{1}$$

and a square-root function,

$$D_2(z) = D_0\sqrt{1-z/h}, \tag{2}$$

to the estimated stem diameters as a function of the height z from ground. In Eqs. (1) and (2), a_1, a_2, and D_0 are fitting parameters, whereas h denotes the estimated tree height. Note that the fitted models have been parametrized such that the fitted stem diameter is always equal to zero at the top of the tree. For both of the fitted models, the volume of the solid of revolution was calculated and the stem volume V was taken to equal the mean of the obtained volumes, i.e.,

$$V = \frac{\pi}{2}\left(\int_0^h \frac{D_1(z)^2}{4}\mathrm{d}z + \int_0^h \frac{D_2(z)^2}{4}\mathrm{d}z\right). \tag{3}$$

2.6. Reference data

We obtained the reference values for the stem attribute measurements by analyzing point clouds collected with a handheld ZEB Horizon laser scanner system. The ZEB Horizon system incorporates a Velodyne VLP-16 scanner mounted on a rotating arm as shown in Fig. 1, which enables the collection of high-density point clouds of forests (Chen et al., 2019; Balenović et al., 2021; Hyyppä et al., 2020a; Hunčaga et al., 2020; Gollob et al., 2020). Importantly, the ZEB Horizon scanner has an in-built SLAM system ensuring that drifts and distortions in the collected point cloud remain small.

When conducting the measurements with the ZEB Horizon scanner, we covered each of the test sites using a walking pattern containing several loops in order to provide multiple possibilities for loop closure detection and subsequent drift elimination. After the data collection, the raw data was pre-processed using the GeoSLAM Hub (version 6.0.0.) software. To this end, we utilized the default values of the processing parameters: Convergence threshold: 0, Window size: 0, Voxel density: 1, Rigidity: 0, Maximum range: 100 m, Closed Loop. After the pre-processing steps, the resulting point cloud data was exported into LAS-format for further processing. In Fig. 6(a) and (b), we illustrate the resulting point cloud on a small region within the first test site. Importantly, the point cloud covers both the stems and the tops of the trees, as a result of which it is possible to accurately estimate stem diameters, tree heights and stem volumes from the point cloud.

We used the algorithmic workflow described in Hyyppä et al. (2020a) to estimate the DBHs, stem curves and stem volumes of individual trees from the point clouds collected with the ZEB Horizon scanner. Our previous study on the ZEB Horizon system showed that these point cloud processing algorithms can be used to estimate the stem curves of the detected trees with a relative bias of 0–5% and a relative RMSE of 5–10% up to the height of 6 m above the ground level (Hyyppä et al., 2020a). For the stem volume estimates, the corresponding relative bias was 0–6%, and the relative RMSE was 9–12%. Importantly, these estimation errors are several times lower than the errors that have been previously reported for direct stem attribute estimation from ALS or UAVLS point clouds. In Liang et al. (2019), the relative RMSE of stem

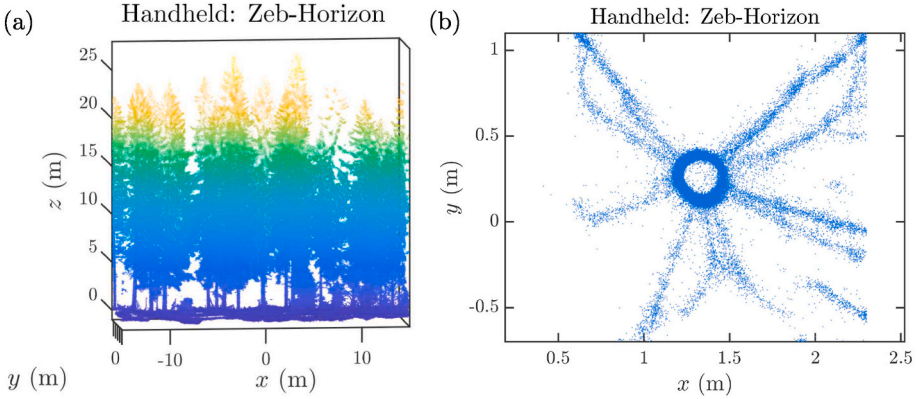

Fig. 6. (a) Point cloud collected with the handheld ZEB Horizon scanner at the test site 1. (b) Stem cross section of an example tree in the point cloud shown in panel (a).

curves estimated from UAVLS data ranged from 30% to 55% depending on the complexity of the boreal forest stand, and the corresponding relative RMSE of stem volume estimates ranged from 50% to over 200%. In Wieser et al. (2017), Brede et al. (2017), Kuželka et al. (2020), and Vandendaele et al. (2021), the RMSE of DBH estimates obtained from UAVLS data varied between 4 cm and 7 cm, which is several times higher than the corresponding RMSE obtained using the ZEB Horizon system (0.9–1.3 cm) in Hyyppä et al. (2020a). Thus, the stem attribute estimates obtained using the ZEB Horizon system are accurate enough to be used as the reference data set for the current study.

Here, we also point out that each of the point clouds produced by the ZEB Horizon scanner was in a local coordinate system since the ZEB Horizon scanner was not equipped with a GNSS receiver. Thus, we utilized the efficient coarse registration algorithm proposed in Hyyppä et al. (2021a) to find the Euclidean transformation mapping the locations of the trees detected from the ZEB Horizon data into the coordinate system of the ALS data. The coarse registration algorithm works by finding the Euclidean transformation between two sets of tree locations without any prior guess for the translation and rotation parameters of the transformation. For each of the test sites, we used the stem locations detected from the ALS point cloud to define the target coordinate system. After transforming the reference stem locations detected from the ZEB Horizon data to the ALS coordinate system, we determined the corresponding reference tree for each of the trees detected from the ALS data by using a distance threshold of 0.4 m in the xy plane.

2.7. Statistical analysis

To assess the accuracy of stem detection from ALS data, we utilized the concepts of completeness and correctness that are defined as

$$\text{Completeness} = \frac{\text{Number of detected reference trees}}{\text{Number of reference trees}} \times 100\%, \tag{4}$$

$$\text{Correctness} = \frac{\text{Number of detected reference trees}}{\text{Number of detected trees}} \times 100\%, \tag{5}$$

where the number of detected reference trees is defined as the number of reference trees with a tree detected from the ALS data within a distance of 0.4 m from the reference tree.

On the other hand, the accuracy of the estimated stem attributes was evaluated using the concepts of bias and RMSE that are given by the following equations

$$\text{bias} = \sum_{i=1}^{N} \frac{x_i - x_{i,\text{ref}}}{N}, \tag{6}$$

$$\text{RMSE} = \sqrt{\sum_{i=1}^{N} \frac{(x_i - x_{i,\text{ref}})^2}{N}}, \tag{7}$$

where N denotes the number of detected reference stems, $\{x_i\}_{i=1}^{N}$ denotes the stem attribute estimates, such as DBH, obtained from the ALS data, and $\{x_{i,\text{ref}}\}_{i=1}^{N}$ denotes the reference values for the stem attribute. In addition, we utilized the relative bias and RMSE that are defined as

$$\text{rbias} = \frac{\text{bias}}{\bar{x}} \times 100\%, \tag{8}$$

$$\text{rRMSE} = \frac{\text{RMSE}}{\bar{x}} \times 100\%, \tag{9}$$

where $\bar{x} = \sum_{i=1}^{N} x_{i,\text{ref}}/N$ denotes the mean value of the reference stem attributes.

When it comes to the stem curve estimates, we evaluated the bias and RMSE using a slightly different approach since each detected tree typically had stem diameter estimates at multiple different heights. Thus, we computed the bias and RMSE of stem curve estimates as

$$\text{bias} = \frac{1}{N} \sum_{i=1}^{N} \sum_{j=1}^{N_i} \frac{D_i(z_j) - D_{i,\text{ref}}(z_j)}{N_i}, \tag{10}$$

$$\text{RMSE} = \sqrt{\frac{1}{N} \sum_{i=1}^{N} \sum_{j=1}^{N_i} \frac{(D_i(z_j) - D_{i,\text{ref}}(z_j))^2}{N_i}}, \tag{11}$$

where $D_i(z_j)$ denotes the estimated stem diameter at the height of z_j for the ith stem detected from the ALS data, $D_{i,\text{ref}}(z_j)$ is the corresponding reference diameter, and N_i denotes the number of reference diameter estimates used for the comparison in the case of the ith tree.

3. Results and discussion

In this section, we present the results regarding ALS-based stem detection and stem attribute estimation for the scenario *high-quality trees*. The results for the scenario *as many trees as possible* are provided in Appendix A.

3.1. Completeness and correctness of stem detection

In this section, we provide results for the completeness and correctness of ALS-based stem detection when considering the results for the scenario *high-quality trees* (see Secs. 2.1 and 2.5.2). As can be seen from Fig. 7(a), the overall completeness rate of stem detection varied between 41.6% and 71.3% on the three test sites. Importantly, Fig. 7(a) also shows the completeness rates computed for four different DBH categories corresponding to stems satisfying DBH $\in [0, 20)$ cm, DBH $\in [20, 30)$ cm, DBH $\in [30, 40)$ cm, and DBH $\in [40, \infty)$ cm. On all of the test sites, the completeness rate was only 20–30% for stems with a DBH smaller than 20 cm, whereas it was significantly higher, i.e., 50–100% for stems with a DBH exceeding 20 cm. The low completeness rate of small trees was caused by the low number of stem hits in the point cloud attributable to the small stem size. Additionally, we point out that one should not draw too far-reaching conclusions for the category DBH $\geq$40 cm since only a small number of trees had a DBH exceeding 40 cm as visualized in Fig. 7(b).

The differences in the completeness rates between the different test sites were also significant since the overall completeness rates were 71.3%, 64.5%, and 41.6% at the test sites 1, 2, and 3, respectively. The low completeness rate at the test site 3 can be partly explained by the large proportion of trees with a DBH smaller than 20 cm. Based on Fig. 7 (a), it is, however, evident that the completeness rate of large trees was also significantly lower at the test site 3 than on the two other test sites. This may have been caused by occlusion arising from the high stem density of the test site 3 (see Table 1). On the other hand, the difference in the completeness rates between the test sites 1 and 2 was probably caused by the point density being almost twice as high in the point cloud of the test site 1 as compared with the point cloud of the test site 2.

The results for the completeness and correctness of stem detection have been summarized in Table 3. Based on our analysis, the correctness rate was 99.0% for the test site 1, 96.8% for the test site 2, and 99.6% for the test site 3. The high level of correctness means that almost all of the stems detected from the ALS data could be associated with a stem detected from the ZEB Horizon data. We point out that the few trees without a matching reference tree may have been actual trees that were not detected from the ZEB Horizon data or they may have been other vertically-oriented objects that were misinterpreted as trees.

In Fig. 8, we show the percentage of trees, for which at least one reliable arc was detected in a given 1-m height interval, as a function of the height from the ground. From the figure, we can observe that the probability for detecting an arc was the highest at 2 m above the ground level even though the point density decreased when approaching the ground level as shown in Fig. 2(d). This may be explained by two factors: First, the stem diameters decreased as a function of the height from the ground reducing the probability for arc detection as discussed above.

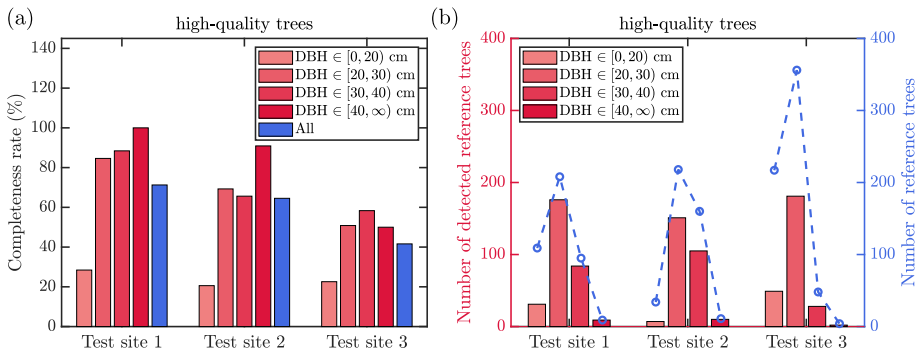

Fig. 7. (a) Completeness rates of stem detection on the three test sites for the scenario *high-quality trees*. In addition to showing the overall completeness rate (blue bar), we also present the completeness rates for four disjoint DBH categories: DBH $\in [0, 20)$ cm, DBH $\in [20, 30)$ cm, DBH $\in [30, 40)$ cm, and DBH $\in [40, \infty)$ cm. (b) Number of detected reference trees and the total number of reference trees in the different DBH categories on the three test sites. (For interpretation of the references to color in this figure legend, the reader is referred to the Web version of this article.)

Table 3
Completeness and correctness rates on the three test sites for ALS-based stem detection for the scenario *high-quality trees*. In addition to the overall completeness rate, we also report the completeness of stem detection for four disjoint DBH categories: DBH $\in [0, 20)$ cm, DBH $\in [20, 30)$ cm, DBH $\in [30, 40)$ cm, and DBH $\in [40, \infty)$ cm. Note that the number of reference stems is based on the number of stems detected from the ZEB Horizon data.

	Completeness (%)					**Correctness (%)**
	Overall	DBH $\in [0, 20)$ cm	DBH $\in [20, 30)$ cm	DBH $\in [30, 40)$ cm	DBH $\in [40, \infty)$ cm	Overall
Test site 1	71.3 (300/421)	28.4 (31/109)	84.6 (176/208)	88.4 (84/95)	100 (9/9)	99.0 (300/303)
Test site 2	64.5 (273/423)	20.6 (7/34)	69.3 (151/218)	65.6 (105/160)	90.9 (10/11)	96.8 (273/282)
Test site 3	41.6 (260/625)	22.6 (49/217)	50.8 (181/356)	58.3 (28/48)	50.0 (2/4)	99.6 (260/261)

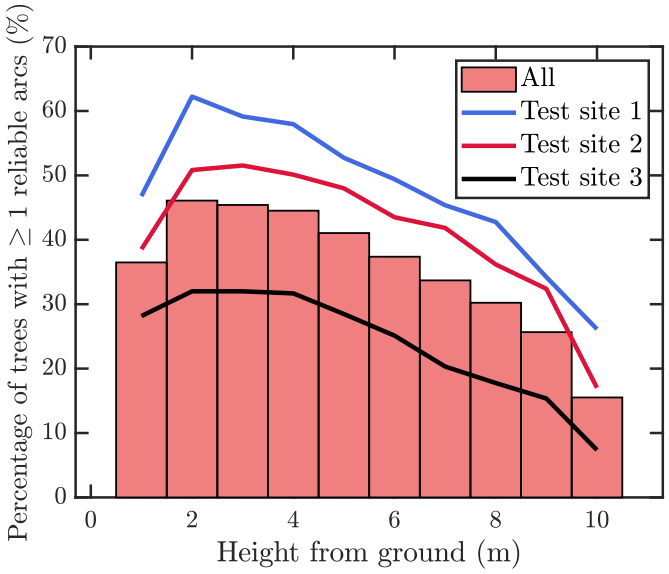

Fig. 8. Proportion of trees, for which at least one reliable arc was detected in a given 1-m height interval, as a function of the height from ground for the scenario *high-quality trees*. The blue line corresponds to the test site 1, the red line corresponds to the test site 2, and the black line corresponds to the test site 3. The solid red bars depict the average for the three test sites. (For interpretation of the references to color in this figure legend, the reader is referred to the Web version of this article.)

Second, the number of branches and needles increased as a function of the height from ground. Thus, reliable arcs were most likely to be detected close to the ground level even though the point density increased as a function of height from the ground.

3.2. Accuracy of measured stem attributes

In this section, we assess the accuracy of the ALS-derived DBHs, stem curves, and stem volumes for the scenario *high-quality trees*. We have summarized the bias and RMSE of the estimated stem attributes for each of the test sites in Tables 4 and 5. The tables also include the bias and RMSE evaluated for each of the four DBH categories introduced in the previous section.

When it comes to the ALS-derived DBHs, the coefficient of determination R^2 varied between 0.69 and 0.88 on the three test sites as illustrated in Fig. 9(a)-(c). As shown in Fig. 10(a), the overall relative bias of DBH estimation was close to zero on all of the test sites, even though the bias showed a slight decreasing trend as a function of the DBH. As shown in Fig. 10(b), the RMSE of the estimated DBHs was 2.2–2.9 cm, i.e., 8.1–9.8%, when trees from all the size categories were considered. The relative RMSE was typically slightly larger for trees in the category DBH <20 cm, but otherwise no clear trends of the RMSE can be distinguished across the different DBH categories.

For the stem curve estimates, the coefficient of determination R^2 was slightly higher, i.e., 0.74–0.91, than the coefficient of determination for the DBH estimates. This is illustrated in Fig. 9(d)–(f). From Fig. 11(a), we see that the relative bias of the stem curve estimates was approximately zero for the test sites 1 and 3, whereas it was −4.2% for the test site 2. Importantly, the overall RMSE of the stem curve estimates ranged from 1.7 cm (6.4%) to 2.6 cm (9.3%) meaning that the RMSE was equivalent or smaller than that of the DBH estimates. In analogy to the RMSE of the DBH estimates, the relative RMSE of the stem curve estimates was the largest for trees in the category DBH <20 cm, whereas the relative RMSE did not vary much as a function of DBH for trees with a DBH exceeding 20 cm. To exemplify the ALS-derived stem curves, we show two example stem curves in Fig. 12. The stem curve shown in Fig. 12(a) belongs to a small tree in the DBH category DBH <20 cm, whereas the stem curve depicted in Fig. 12(b) belongs to a relatively large tree, the DBH of which falls into the interval $[30, 40)$ cm. On average, the stem curve could be estimated for heights in the range of $z \in [1.5, 8.0]$ m.

When it comes to the stem volumes estimated from the ALS point clouds, the coefficient of determination R^2 varied between 0.83 and 0.94 as illustrated in Fig. 9(g)–(i). From Fig. 13(a), we see that the overall bias of the stem volume estimates varied between − 9.3% (test site 2) and 5.8% (test site 3). The relatively large negative bias at the test site 2 was caused by the underestimation of the stem curves that were utilized to compute the stem volume. Fig. 13(b) shows that the overall relative RMSE of the stem volume estimates ranged from 12.7% at the test site 1 to 21.3% at the test site 3. The relative RMSE was markedly larger for

Table 4
Bias and RMSE of DBH and stem curve estimates on the three test sites for the scenario *high-quality trees*. In addition to the overall bias and RMSE, we also report the bias and RMSE for each of the four DBH categories.

	DBH				Stem curve			
	bias	rbias	RMSE	rRMSE	bias	rbias	RMSE	rRMSE
Test site 1								
Overall	0.3 cm	1.2%	2.2 cm	8.1%	−0.1 cm	−0.4%	1.7 cm	6.4%
DBH ∈ [0, 20) cm	0.8 cm	4.8%	1.6 cm	9.2%	0.4 cm	2.5%	1.6 cm	9.5%
DBH ∈ [20, 30) cm	0.6 cm	2.4%	1.9 cm	7.8%	−0.0 cm	−0.1%	1.5 cm	6.3%
DBH ∈ [30, 40) cm	−0.2 cm	−0.7%	2.4 cm	7.1%	−0.4 cm	−1.4%	1.8 cm	5.7%
DBH ∈ [40, ∞) cm	−1.8 cm	−4.3%	4.9 cm	11.4%	−0.2 cm	−0.7%	1.4 cm	7.3%
Test site 2								
Overall	−0.2 cm	−0.7%	2.9 cm	9.8%	−1.2 cm	−4.2%	2.6 cm	9.3%
DBH ∈ [0, 20) cm	2.2 cm	11.4%	2.9 cm	15.3%	−0.7 cm	−3.2%	2.6 cm	12.6%
DBH ∈ [20, 30) cm	0.3 cm	1.0%	2.2 cm	8.4%	−1.1 cm	−4.3%	2.4 cm	9.5%
DBH ∈ [30, 40) cm	−0.7 cm	−2.1%	3.4 cm	10.1%	−1.3 cm	−4.0%	2.8 cm	8.9%
DBH ∈ [40, ∞) cm	−3.4 cm	−8.2%	2.6 cm	12.2%	−2.3 cm	−5.9%	3.5 cm	9.1%
Test site 3								
Overall	0.3 cm	1.4%	2.3 cm	9.6%	0.1 cm	0.6%	1.9 cm	8.2%
DBH ∈ [0, 20) cm	1.2 cm	6.6%	2.2 cm	12.2%	0.6 cm	3.4%	1.8 cm	10.3%
DBH ∈ [20, 30) cm	0.1 cm	0.6%	2.3 cm	9.2%	0.0 cm	0.1%	1.9 cm	7.9%
DBH ∈ [30, 40) cm	0.2 cm	0.6%	3.0 cm	9.4%	0.3 cm	0.9%	2.3 cm	7.7%
DBH ∈ [40, ∞) cm	−1.6 cm	−3.8%	2.2 cm	5.3%	−1.3 cm	−3.4%	1.4 cm	3.7%

Table 5
Bias and RMSE of stem volume estimates on the three test sites for the scenario *high-quality trees*. In addition to the overall bias and RMSE, we also report the bias and RMSE for each of the four DBH categories.

	Stem volume			
	bias	rbias	RMSE	rRMSE
Test site 1				
Overall	17 dm^3	2.2%	96 dm^3	12.7%
DBH ∈ [0, 20) cm	44 dm^3	16.0%	86 dm^3	31.1%
DBH ∈ [20, 30) cm	13 dm^3	2.2%	82 dm^3	13.3%
DBH ∈ [30, 40) cm	5 dm^3	0.5%	117 dm^3	10.4%
DBH ∈ [40, ∞) cm	101 dm^3	6.1%	149 dm^3	9.0%
Test site 2				
Overall	−88 dm^3	−9.3%	146 dm^3	15.4%
DBH ∈ [0, 20) cm	−82 dm^3	−17.3%	134 dm^3	28.2%
DBH ∈ [20, 30) cm	−78 dm^3	−10.2%	126 dm^3	16.4%
DBH ∈ [30, 40) cm	−95 dm^3	−8.2%	160 dm^3	13.9%
DBH ∈ [40, ∞) cm	−164 dm^3	−9.0%	247 dm^3	13.5%
Test site 3				
Overall	31 dm^3	5.8%	116 dm^3	21.3%
DBH ∈ [0, 20) cm	48 dm^3	18.6%	162 dm^3	62.4%
DBH ∈ [20, 30) cm	19 dm^3	3.5%	93 dm^3	16.9%
DBH ∈ [30, 40) cm	78 dm^3	8.6%	150 dm^3	16.5%
DBH ∈ [40, ∞) cm	43 dm^3	2.4%	73 dm^3	4.1%

small trees in the category DBH ∈ [0, 20) cm, which can be attributed to two factors: First, the relative RMSE of the stem curve estimates was larger for trees in the category DBH ∈ [0, 20) cm than for trees with a DBH >20 cm. Second, the heights of small trees were sometimes overestimated whenever they were growing close to neighboring dominant trees. Based on our results, the relative RMSE decreased slightly as a function of the tree size also for trees with a DBH exceeding 20 cm, and consequently, the RMSE of the stem volume estimates was as low as 4.1–13.5% in the category DBH ∈ [40, ∞) cm.

3.3. Further discussion

As explained in Sec. 2.6, the reference data for this study was based on stem information extracted automatically from the point clouds collected with a handheld ZEB Horizon system. Therefore, it is possible that the actual number of trees at the test sites may have been slightly higher than the number of reference trees we used to compute the statistics. In one of our previous studies (Hyyppä et al., 2020a), the completeness of stem detection for the ZEB Horizon system varied between 77% and 93% on two test sites located in a boreal forest. Nevertheless, we can still conclude that approximately half of the stems could be detected from the ALS point clouds even if strict quality criteria were used for the stem detection in order to obtain highly accurate stem curve estimates. When it comes to the scenario *as many trees as possible* (see Appendix A), our results indicate that it is possible to detect almost as many stems (85–100%) from the ALS point clouds as can be detected from data collected with a ZEB Horizon system provided that one is interested in trees with a DBH exceeding 20 cm.

Subsequently, we briefly discuss potential applications for the scenarios *high-quality trees* and *as many trees as possible*. The algorithm parameters for the scenario *high-quality trees* were chosen to provide highly accurate stem curve estimates (RMSE = 6–9%) and stem volume estimates (RMSE = 12–21%) for a sufficiently large proportion of the trees. In principle, these accurate stem attribute estimates could be used to construct a training data set for teaching machine learning models needed in a large-scale forest inventory at the individual tree level. For this application, the accuracy of the obtained stem attributes should be prioritized over the completeness rate of the stem detection. This is for the reason that the training data set only needs to contain a representative sample of the trees within the large area to be inventoried instead of containing most or all of the trees on some specific reference test sites (Puliti et al., 2020). To ensure that the reference trees correspond to a representative sample, one may need to sample the trees detected from the ALS data according to the DBH-dependent detection rates since our results in Sec. 3.1 suggest that the completeness rate was significantly lower for trees with a DBH <20 cm than for trees with a DBH exceeding 20 cm. If the forest inventory focuses on log trees with DBH ≥20 cm, e.g., due to their economic value, the sampling step is not necessary since the completeness rate did not vary much for trees with a DBH exceeding 20 cm.

When it comes to the scenario *as many trees as possible*, our results in Appendix A indicate that it is possible to detect 85–100% of the trees with a DBH ≥20 cm, where the number of reference trees represents the number of stems detected from the ZEB Horizon data. Thus, the scenario *as many trees as possible* corresponds to conducting a small-scale forest inventory at the individual tree level for medium-sized and large trees. For such a small-scale forest inventory, one can directly use the stem curves and volumes estimated from the relatively dense ALS point clouds without the need to collect less dense ALS data from the area to be inventoried. Naturally, the average errors for the stem curves and volumes were slightly larger for the scenario *as many trees as possible* as compared with the scenario *high-quality trees*. Namely, the RMSE of stem curves was 9–12% and the RMSE of stem volumes was 17–29%. Despite

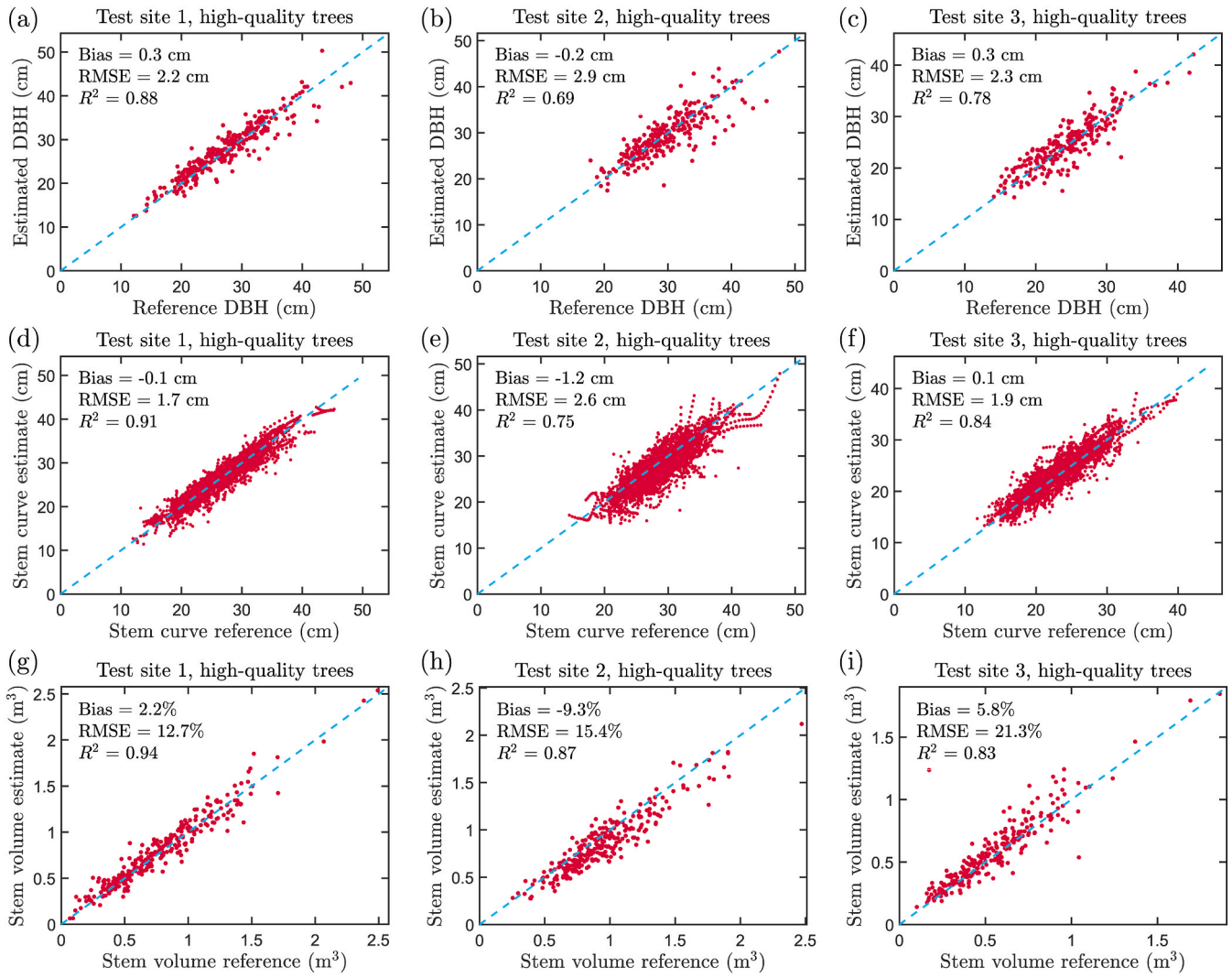

Fig. 9. Scatter plots for DBH, stem curve and stem volume on the three test sites for the scenario *high-quality trees*. (a–c) Scatter plots for the DBHs measured directly from the ALS data vs the reference DBHs at the test sites 1, 2, and 3, respectively. (d–f) Scatter plots for the stem curve estimates measured from the ALS data vs the reference stem curves at the test sites 1, 2, and 3, respectively. (g–i) Scatter plots for the stem volumes measured directly from the ALS data vs the reference stem volumes at the test sites 1, 2, and 3, respectively. In all of the panels, the dashed blue line corresponds to $y = x$. (For interpretation of the references to color in this figure legend, the reader is referred to the Web version of this article.)

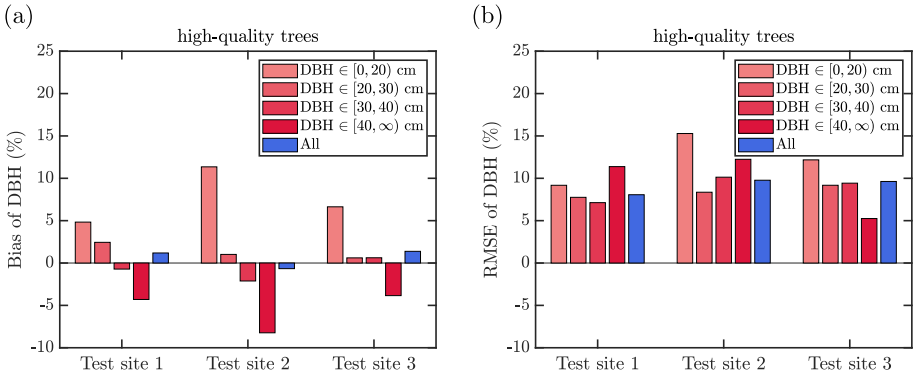

Fig. 10. Relative (a) bias and (b) RMSE of DBH estimates on the three test sites for the scenario *high-quality trees*. We show both the overall bias and RMSE (blue bars) as well as the bias and RMSE for each of the four DBH categories (red bars). (For interpretation of the references to color in this figure legend, the reader is referred to the Web version of this article.)

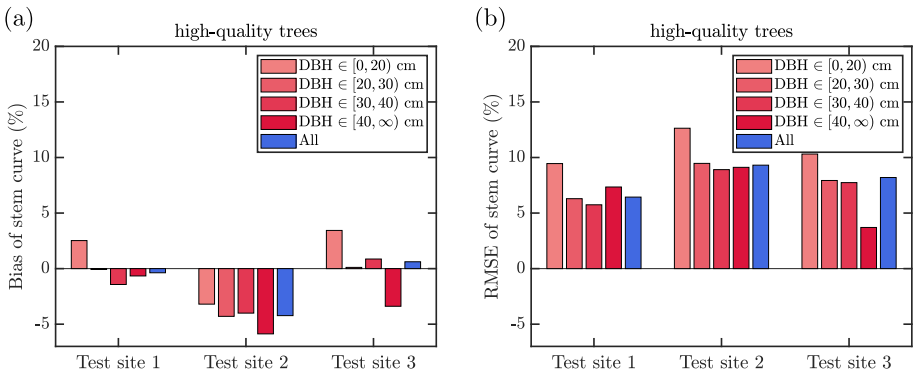

Fig. 11. Relative (a) bias and (b) RMSE of stem curve estimates on the three test sites for the scenario *high-quality trees*. We show both the overall bias and RMSE (blue bars) as well as the bias and RMSE for each of the four DBH categories (red bars). (For interpretation of the references to color in this figure legend, the reader is referred to the Web version of this article.)

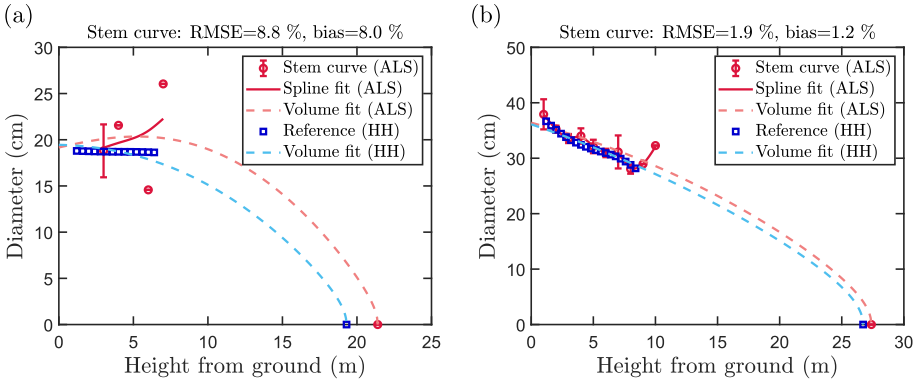

Fig. 12. (a) Example of an estimated stem curve for a tree in the category DBH ∈ [0, 20) cm. (b) Example of an estimated stem curve for a tree in the category DBH ∈ [30, 40) cm. In both of the panels, the red circles illustrate the stem diameters estimated directly from the ALS point cloud, the solid red line is a smoothing spline fit to the diameter estimates, and the blue squares depict the reference stem curves. The dashed lines have been obtained via the equation $D(z) = \sqrt{(D_1(z)^2 + D_2(z)^2)/2}$ (See Eqs. (1) and (2)) and they illustrate the effective diameters for the solids of revolution that were used to compute the stem volume. (For interpretation of the references to color in this figure legend, the reader is referred to the Web version of this article.)

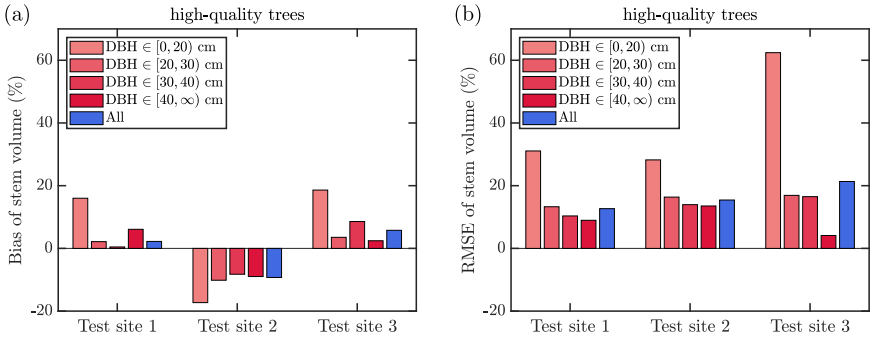

Fig. 13. Relative (a) bias and (b) RMSE of stem volume estimates on the three test sites for the scenario *high-quality trees*. We show both the overall bias and RMSE (blue bars) as well as the bias and RMSE for each of the four DBH categories (red bars). (For interpretation of the references to color in this figure legend, the reader is referred to the Web version of this article.)

of the different completeness rates, the correctness of stem detection differed only by one percent between the scenarios *as many trees as possible* and *high-quality trees*.

Subsequently, we compare the accuracy of our results to previous studies that have used high-density ALS data for deriving direct stem attribute estimates for individual trees. In Liang et al. (2019), the RiCOPTER system (Riegl GmbH, Austria) was used to measure the DBHs, stem curves, and stem volumes of individual trees in 24 boreal forest test sites classified as easy, medium-difficult or difficult. Depending on the difficulty of the test site, the relative RMSE of DBH estimates ranged from 20% to 50%, the RMSE of stem curve estimates ranged from 30% to 55% and the RMSE of stem volume estimates ranged from 60% to 225%. Brede et al. (2017) also utilized the RiCOPTER system to study DBH estimation from an airborne platform in 5 different test sites representing different forest types. Based on 39 tree stems, they obtained an RMSE of 4.2 cm for the DBH estimates when using TLS data as the reference. In Wieser et al. (2017), the RiCOPTER system was used to study DBH estimation on 6 plots. Based on 57 detected stems, an RMSE of 7.5 cm was obtained for the DBH estimates but the RMSE could be reduced down to 1.9 cm if four gross outliers were excluded from the analysis. In the studies by Wieser et al. and by Brede et al., manual point selection was performed to choose the points for the DBH estimation. Kuželka et al. (2020) obtained an RMSE of 6.0 cm, i.e., 19% for DBH estimation by using ALS data collected with the RiCOPTER system. Kuzelka et al. also measured the stem curves for the detected trees, but they could not assess the accuracy of the stem curve estimates due to a lack of reference data. Most recently, Vandendaele et al. (2021) obtained an RMSE of 7.4 cm for DBH estimation by using a Velodyne HDL-32E

Table 6
Comparison of our results to previous studies that have used high-density ALS or UAVLS data to conduct direct measurements of DBH and other stem attributes of individual trees. For each study, we report the laser scanning system, flight altitude above the ground level, point density of the resulting point cloud(s), completeness of tree detection, and RMSE for DBH, stem curve and stem volume estimates. Importantly, the completeness rates are not fully comparable between the different studies since manual selection of trunk points was used in Brede et al. (2017) and Wieser et al. (2017), and thus, the completeness rates refer to the success rate of circle/cylinder fitting for these two studies.

		Altitude	Density	Completeness	RMSE (absolute or relative)		
Study	System	(m)	(pts/m^2)	(%)	DBH	Stem curve	Stem volume
Wieser et al. (2017)	RiCOPTER	50	1500	81	7.5 cm	–	–
Brede et al. (2017)	RiCOPTER	90	3000–5300	67	4.2 cm	–	–
Liang et al. (2019)	RiCOPTER	50	4000–18000	20–60	20–50%	30–55%	60–225%
Kuželka et al. (2020)	RiCOPTER	100	2000	98–99	6.0 cm	–	–
Vandendaele et al. (2021)	Velodyne HDL-32E on a UAV	40	1585	71	7.4 cm	–	–
Ours (*high-quality trees*)	RieglVUX-1HA on a helicopter	80	2200–3800	42–71	2.2–2.9 cm 8.1–9.8%	1.7–2.6 cm 6.4–9.3%	96-146 dm^3 12.7–21.3%
Ours (*as many trees as possible*)	RieglVUX-1HA on a helicopter	80	2200–3800	72–90	2.6–3.5 cm 10.1–14.6%	2.2–2.8 cm 9.0–12.4%	122-180 dm^3 17.7–29.3%

scanner mounted on a UAV. Vandendaele et al. were able to detect 71% of the trees automatically using the SimpleTree (Hackenberg et al., 2015) library that was originally developed for analysing forest data collected with a TLS system.

We have summarized the key results of the above-mentioned previous studies and our current study in Table 6. Based on the table, the RMSE values obtained in the current study are far more precise than in any of the previous studies, whereas the completeness rate of stem detection remains comparable to the previous studies. Importantly, we were able to derive the stem curve and volume with a high accuracy for each detected tree unlike in any of the previous studies. The point density in the current study was of similar order of magnitude as in the previous studies. This suggests that the accuracy improvements can be attributed at least partly to the use of algorithms that are robust against distortions arising from the slow drifts in the trajectory of the laser scanner. In the previous studies, the stem diameters have namely been estimated using methods that are similar to algorithms designed for analyzing static TLS data. When it comes to the scenario *high-quality trees*, the obtained RMSE values for the stem curve and volume estimates were not much larger than the RMSE values that have been obtained with ground-based MLS systems in comparable boreal forest conditions. In Hyyppä et al. (2020a), the RMSE of stem volume estimates varied between 9% and 15% for handheld, backpack, and under-canopy UAV laser scanning systems depending on the complexity of the forest conditions and the data acquisition method.

Finally, we briefly address the scalability of our approach. The flight time required to collect the ALS data was approximately 10–15 min for each of the test sites. Importantly, the resulting point clouds covered a much larger region than just the test site. As an example, the point cloud collected over the first test site had a sufficiently high point density for the detection of approximately 6000 stems across an area of 21 ha. In theory, it is thus possible to use a similar ALS system for collecting reference data for roughly 500 trees per minute. In our current implementation, the time taken by the point cloud processing limits the speed of ALS-based reference data collection. Namely, it takes approximately 0.5–3 h to process 1 ha of the point cloud resulting in approximately 400 detected trees. We ran the code implemented in Matlab on a laptop with Intel Core i7-7820HQ 2.9 GHz processor and 32 GB of RAM. In the future, the speed of data processing may be improved by using multiple cores or computers to explicitly parallelize the data processing, by using a programming language targeted for high-performance computing, such as C++, and by reducing the number of high-resolution images saved for each detected tree.

4. Conclusions

In this paper, we studied the use of high-density ALS point clouds for accurate and direct stem curve and volume measurements at the individual tree level. To this end, we collected point cloud data on three test sites located in a boreal forest using an in-house developed helicopter-based HeliALS-DW system incorporating a Riegl VUX-1HA scanner. Importantly, the scanner was tilted 15° with respect to the vertical direction to obtain a high number of stem hits with the laser beam. To collect point clouds with a relatively high point density of 2200–3800 pt/m^2, the test sites were covered with a square grid pattern, and the flights were carried out using a low flight altitude of 80 m. For the stem curve estimation, we used algorithms that were robust against point cloud distortions caused by slow drifts and subsequent local mismatches in the trajectory of the scanner. To obtain high-quality stem volume estimates, we used the estimated stem curves and tree heights in order to compute the stem volume instead of using national allometric models for predicting the stem volume from the DBH and the tree height.

In our analysis, we investigated two scenarios named as *high-quality trees* and *as many trees as possible*. In the scenario *high-quality trees*, we used strict quality criteria in the stem curve estimation algorithm with the goal of obtaining accurate stem curve and volume estimates for field reference trees at the test sites. In the scenario *as many trees as possible*, we used more lenient quality criteria in order to detect most of the trees with the cost of increased average errors. The completeness rate of stem detection varied between 41.6% and 71.3% for the scenario *high-quality trees*, whereas the completeness rate was 72.2–89.5% for the scenario *as many trees as possible* reaching 86.5–96.5% for trees with a DBH exceeding 20 cm. The completeness rate was significantly reduced for trees with a DBH smaller than 20 cm, whereas most of the trees with a DBH exceeding 20 cm could be largely detected in both of the scenarios. Based on our results, the RMSE of stem curve estimates was 1.7–2.6 cm, i.e., 6.4–9.3%, for the scenario *high-quality trees* and 2.2–2.9 cm, i.e., 9.0–12.4%, for the scenario *as many trees as possible*. When it comes to the stem volume estimates, the RMSE was 12.7–21.3% for the scenario *high-quality trees* and 17.7–29.3% for the scenario *as many trees as possible*. Importantly, the RMSE values obtained for the DBH, stem curve and stem volume were far smaller than in the previous studies in the literature investigating direct stem diameter measurements from high-density ALS or UAVLS data. Furthermore, the average errors obtained in the current study were not much larger than the errors that have been previously obtained with ground-based MLS systems, such as backpack laser scanning, in comparable boreal forest conditions.

The use of ALS or UAVLS systems for reference data collection would have the following benefits: First, the point clouds are easily georeferenced thanks to a strong GNSS signal above the forest canopy. Second, the speed of reference data collection would be unprecedented since point cloud data covering tens of thousands of trees could be collected during a single day. Third, tree height measurements are more accurate from point cloud data collected with an above-canopy flying platform.

The downsides of the proposed approach include the increased costs of the laser scanning equipment due to high precision requirements and the slightly reduced quality of the point cloud, both of which are caused by the long range between the laser scanner and the tree stems to be modeled.

In the future, the capability of direct ALS measurements for reference data collection should be verified by using the estimated stem attributes to train prediction models needed in an individual-tree-level forest inventory. By comparing the inventory results to those obtained when standard field measurements are used as the reference data, one could conclude whether the stem attribute estimates obtained from high-density ALS data are sufficiently accurate for operational applications. Furthermore, more research would be needed to test and develop the sampling strategies, flight operations and point cloud processing methods in more complex forest conditions and in different types of forests. In conclusion, our results present an important step towards utilizing high-density ALS or UAVLS data for highly-efficient reference data collection at the individual tree level.

Author contributions

E.H. developed the algorithms for stem curve and volume estimation, and analyzed the ALS data. A.K. designed and built the scanning system. A.K., T.H. and H.K. planned and performed the laser scanning measurements for the study. The reference data collected with the ZEB Horizon system was analyzed by X.Y. and J.M. The experiment design was done by E.H., A.K. and J.H. The paper was written by E.H., and J.H, assisted by A.K., H.K., X.Y., J.M, and T.H. Funding was organized by J. H., E.H. (co-writing of applications) and A.K. J.H and A.K. were senior authors.

Declaration of interests

The authors declare that they have no known competing financial interests or personal relationships that could have appeared to influence the work reported in this paper.

Funding information

We gratefully acknowledge Academy of Finland that funded this research through grants “Forest-Human-Machine Interplay - Building Resilience, Redefining Value Networks and Enabling Meaningful Experiences (337656)”, “Estimating Forest Resources and Quality-related Attributes Using Automated Methods and Technologies” (334829, 334830), “Feasibility of Inside-Canopy UAV Laser Scanning for Automated Tree Quality Surveying” (334002), “Capturing structural and functional diversity of trees and tree communities for supporting sustainable use of forests” (348644), Mapping of forest health, species and forest fire risks using Novel ICT Data and Approaches (344755) and Ministry of Agriculture and Forestry that funded this research through the grant “Future forest information system at individual tree level” (VN/3482/2021). Academy-funded research infrastructure grant “Measuring Spatiotemporal Changes in Forest Ecosystem” (336382) was also applied in this study. Prof. Mikko Vastaranta, University of Eastern Finland, is acknowledged as a key collaborator in this research infrastructure project.

Appendix. A Results for the scenario *as many trees as possible*

In this appendix, we present the results regarding stem detection and stem attribute estimation when it comes to the scenario *as many trees as possible*. As explained in Sec. 2.5, we used more lenient parameter values in the stem curve estimation algorithm for this scenario than for the scenario *high-quality trees* in order to detect a larger proportion of the trees with the cost of increased errors in the estimated stem attributes.

Appendix. A.1 Completeness and correctness of stem detection

We summarize the results for the completeness of stem detection in Fig. A.1 and in Table A.1. The overall completeness rate ranged from 72.2% for the test site 3 to 89.5% for the test site 1. Similarly to the scenario *high-quality trees*, the completeness rate was the lowest, i.e., 29.4–69.7%, for trees that belonged to the category DBH $\in [0, 20)$ cm. When considering trees with a DBH larger than 20 cm, the completeness rate varied between 86.5% and 96.5% on all of the test sites. For example, the completeness rate at the test site 1 was as high as 95.2% for the category DBH $\in [20, 30)$ cm, and 98.9% for the category DBH $\in [30, 40)$ cm. The high completeness rate at the test site 1 can probably be attributed to the point density of 3800 pt/m^2 that was 70% higher than that for the test site 2 and 30% higher than that for the test site 3.

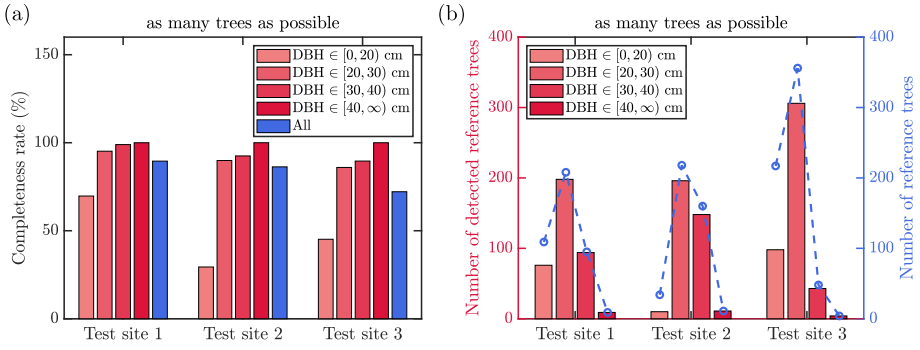

Fig. A.1. (a) Completeness rates of stem detection on the three test sites for the scenario *as many trees as possible*. In addition to showing the overall completeness rate (blue bar), we also present the completeness rates for four disjoint DBH categories: DBH $\in [0, 20)$ cm, DBH $\in [20, 30)$ cm, DBH $\in [30, 40)$ cm, and DBH $\in [40, \infty)$ cm. (b) Number of detected reference trees and the total number of reference trees in the different DBH categories on the three test sites.

In Table A.1, we report the correctness rates of stem detection for all of the test sites. The correctness rate was the lowest for the test site 2, for which 4.5% of the detected trees did not correspond to a reference tree detected from the ZEB Horizon data. Overall, the correctness rates were only one percentage point lower than for the scenario *high-quality trees* even though the more lenient parameter values allowed us to detect a far larger proportion of the trees.

Table A.1
Completeness and correctness rates of ALS-based stem detection on the three test sites for the scenario *as many trees as possible*. In addition to the overall completeness rate, we also report the completeness of stem detection for four disjoint DBH categories: DBH $\in [0, 20)$ cm, DBH $\in [20, 30)$ cm, DBH $\in [30, 40)$ cm, and DBH $\in [40, \infty)$ cm. Note that the number of reference stems is based on the number of stems detected from the ZEB Horizon data.

	Completeness (%)					**Correctness (%)**
	Overall	DBH $\in [0, 20)$ cm	DBH $\in [20, 30)$ cm	DBH $\in [30, 40)$ cm	DBH $\in [40, \infty)$ cm	Overall
Test site 1	89.5 (377/421)	69.7 (76/109)	95.2 (198/208)	98.9 (94/95)	100 (9/9)	97.9 (377/385)
Test site 2	86.2 (365/423)	29.4 (10/34)	89.9 (196/218)	92.5 (148/160)	100 (11/11)	95.5 (365/382)
Test site 3	72.2 (451/625)	45.2 (98/217)	85.9 (306/356)	89.6 (43/48)	100 (4/4)	98.9 (451/456)

In Fig. A.2, we show the percentage of trees, for which at least one reliable arc was detected in a given 1-m height interval, as a function of the height from ground. Similarly to the scenario *high-quality trees*, the probability of arc detection was the highest at the height of $z = 2$ m. By comparing Fig. A.1(a) and Fig. A.2, we can observe that the overall completeness rates significantly exceeded the percentage of trees, for which at least one reliable arc was detected at the height of $z = 2$ m. This suggests that it is beneficial to detect arcs at multiple heights in order to detect as many stems as is possible from the point cloud data. As compared with the scenario *high-quality trees*, there were no significant qualitative differences in the height dependence of the arc detection probability apart from the obvious fact that the arc detection probability was higher throughout the studied height range when using parameter values corresponding to the scenario *as many trees as possible*.

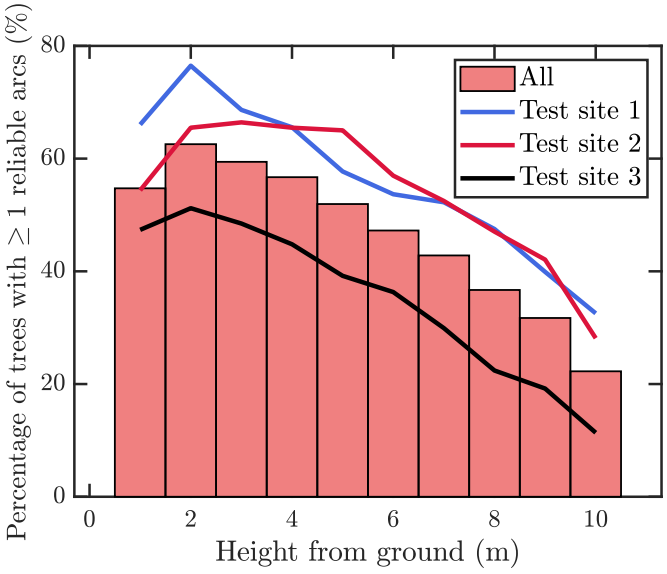

Fig. A.2. Proportion of trees, for which at least one reliable arc was detected in a given 1-m height interval, as a function of the height from ground for the scenario *as many trees as possible*. The blue line corresponds to the test site 1, the red line corresponds to the test site 2, and the black line corresponds to the test site 3. The solid red bars depict the average for the three test sites.

Appendix. A.2 Accuracy of ALS-derived stem attributes

In this section, we present the results for the ALS-derived DBHs, stem curves, and stem volumes when considering the scenario *as many trees as possible*. Tables A.2 and A.3 summarize the bias and RMSE of the estimated stem attributes for each of the test sites. The tables also include the bias and RMSE evaluated for each of the four DBH categories introduced in Sec. 3.1.

For the scenario *as many trees as possible*, the coefficient of determination R^2 of the ALS-derived DBHs varied between 0.63 and 0.86 across the three test sites as illustrated in Fig. A.3(a)–(c). As shown in Fig. A.4(a), the overall relative bias of the DBH estimates was below 4% on all of the test sites. For trees in the category DBH $\in [0, 20)$ cm, the relative bias was, however, substantially above zero and ranged from 7.8% (test site 1) up to 19.5% (test site 2). Based on Fig. A.4(b), the overall relative RMSE of the estimated DBHs was 10.1–14.6%. In the category DBH $\in [0, 20)$ cm, the relative RMSE was markedly higher, and ranged up to 29.3% in the case of the test site 2.

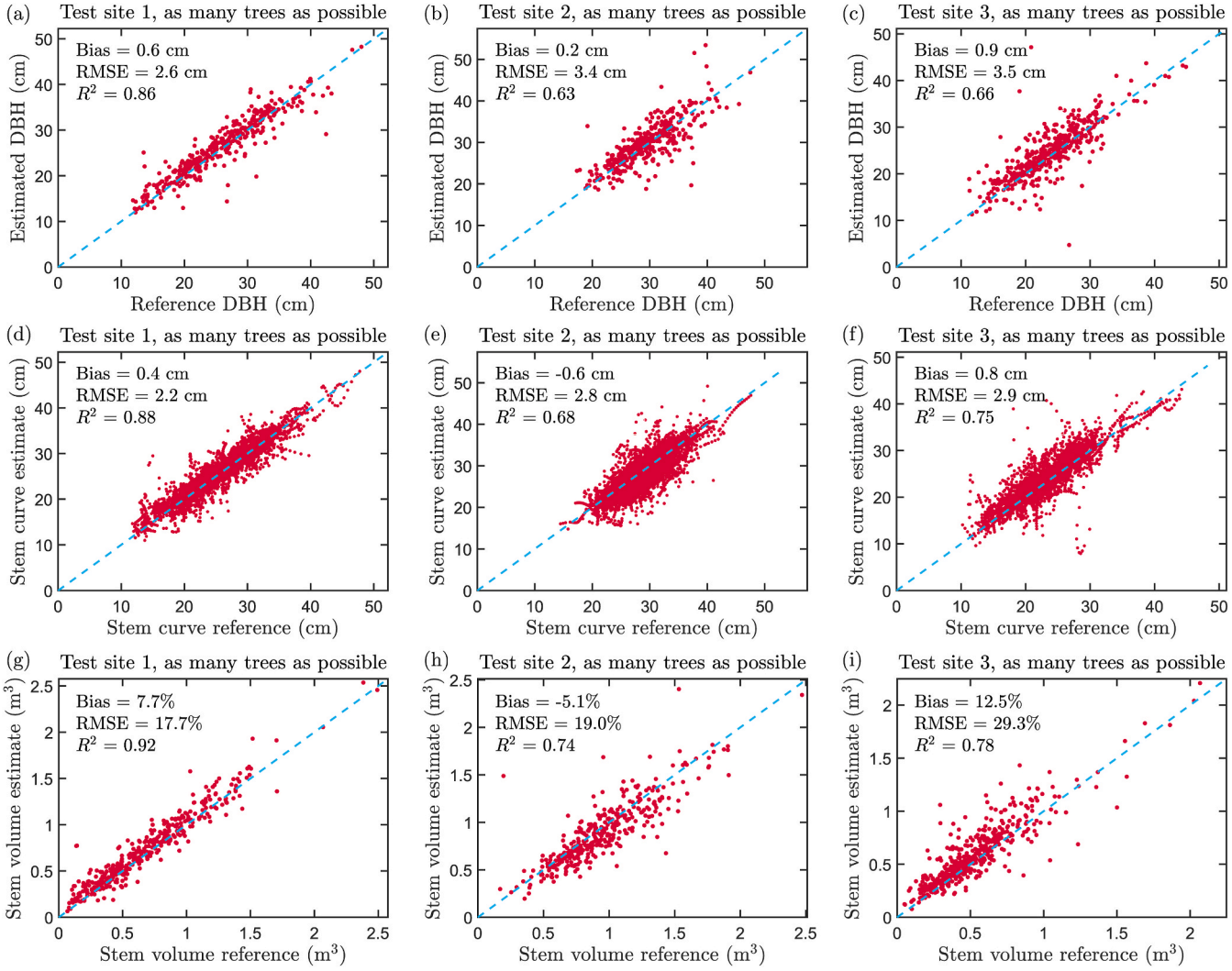

Fig. A.3. Scatter plots for DBH, stem curve and stem volume on the three test sites for the scenario *as many trees as possible*. (a-c) Scatter plots for the DBHs measured directly from the ALS data vs the reference DBHs at the test sites 1, 2, and 3, respectively. (d-f) Scatter plots for the stem curve estimates measured from the ALS data vs the reference stem curves at the test sites 1, 2, and 3, respectively. (g-i) Scatter plots for the stem volumes measured directly from the ALS data vs the reference stem volumes at the test sites 1, 2, and 3, respectively. In all of the panels, the dashed blue line corresponds to $y = x$.

When it comes to the stem curve estimates, the coefficient of determination R^2 varied between 0.68 and 0.88 across the test sites as depicted in Fig. A.3(d)–(f). As shown in Fig. A.5(a), the overall relative bias of the stem curve estimates was close to zero. Importantly, the relative RMSE of the stem curve estimates was slightly lower than the RMSE of the DBH estimates in analogy to the scenario *high-quality trees*. Namely, the overall relative RMSE ranged from 9.0% to 12.5% as illustrated in Fig. A.5(b). Again, the relative RMSE was significantly higher in the category DBH $\in [0, 20)$ cm as compared with the other DBH categories.

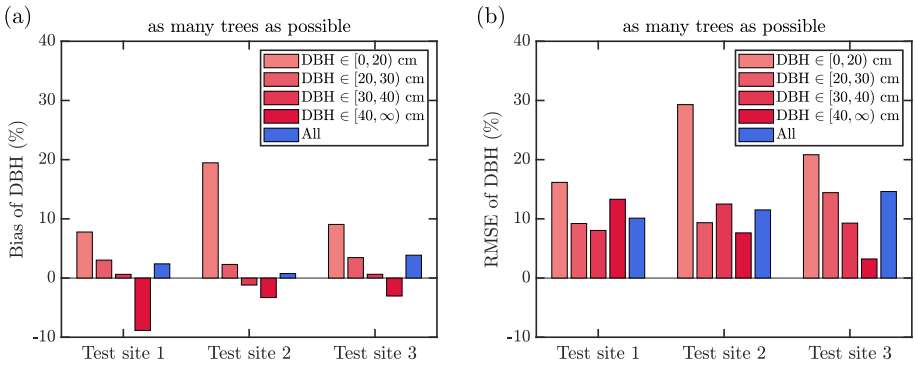

Fig. A.4. Relative (a) bias and (b) RMSE of DBH estimates on the three test sites for the scenario *as many trees as possible*. We show both the overall bias and RMSE (blue bars) as well as the bias and RMSE for each of the four DBH categories (red bars).

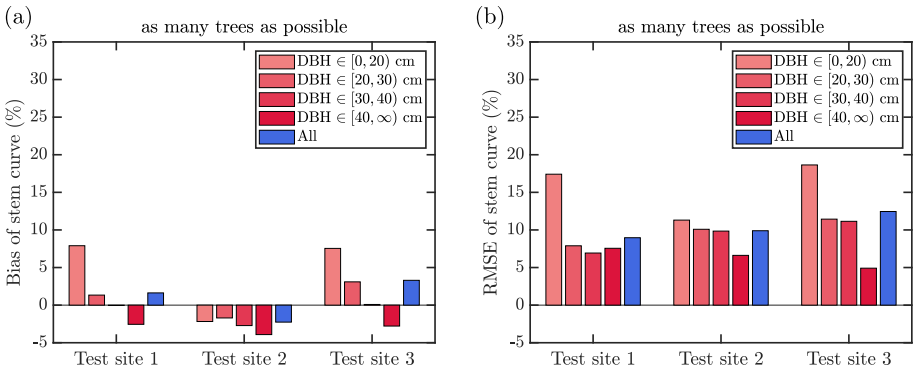

Fig. A.5. Relative (a) bias and (b) RMSE of stem curve estimates on the three test sites for the scenario *as many trees as possible*. We show both the overall bias and RMSE (blue bars) as well as the bias and RMSE for each of the four DBH categories (red bars).

For the stem volume estimates, the coefficient of determination R^2 varied between 0.74 and 0.92 as illustrated in Fig. A.3(g)-(i). Fig. A.6(a) shows that the overall relative bias of the stem volume estimates ranged from −5.1% (test site 2) up to 12.4% (test site 3). Again, the relative RMSE was significantly larger for small trees that belonged to the DBH category DBH $\in [0, 20)$ cm. For these trees, the relative RMSE was as high as 58.8–100.0% depending on the test site. On the other hand, the overall relative RMSE of the stem volume estimates was 17.7–29.3%, and the relative RMSE was as low as 5.3–11.6% for the trees with a DBH exceeding 40 cm.

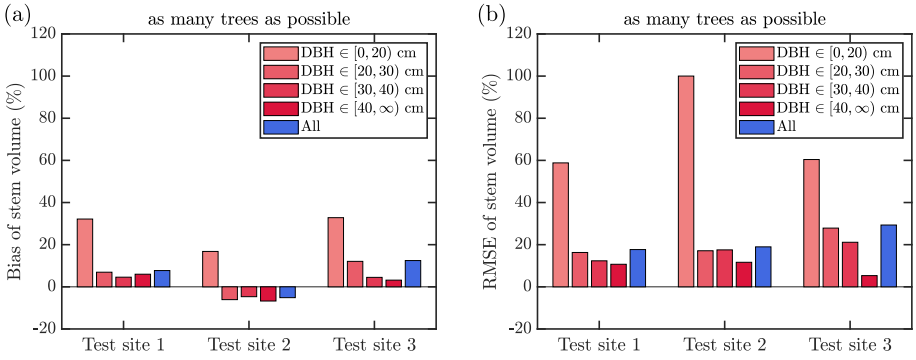

Fig. A.6. Relative (a) bias and (b) RMSE of stem volume estimates on the three test sites for the scenario *as many trees as possible*. We show both the overall bias and RMSE (blue bars) as well as the bias and RMSE for each of the four DBH categories (red bars).

Table A.2
Bias and RMSE of DBH and stem curve estimates on the three test sites for the scenario *as many trees as possible*. In addition to the overall bias and RMSE, we also report the bias and RMSE for each of the four DBH categories.

	DBH				**Stem curve**			
	bias	rbias	RMSE	rRMSE	Bias	rbias	RMSE	rRMSE
Test site 1								
Overall	0.6 cm	2.4%	2.6 cm	10.1%	0.4 cm	1.6%	2.2 cm	9.0%
DBH ∈ [0, 20) cm	1.3 cm	7.8%	2.7 cm	16.2%	1.3 cm	7.9%	2.9 cm	17.4%
DBH ∈ [20, 30) cm	0.7 cm	3.0%	2.3 cm	9.2%	0.3 cm	1.3%	1.9 cm	7.9%
DBH ∈ [30, 40) cm	0.2 cm	0.6%	2.7 cm	8.0%	−0.0 cm	−0.0%	2.2 cm	6.9%

(*continued on next page*)

Table A.2 (*continued*)

	DBH				Stem curve			
	bias	rbias	RMSE	rRMSE	Bias	rbias	RMSE	rRMSE
DBH ∈ [40, ∞) cm	−3.8 cm	−8.8%	5.7 cm	13.3%	−1.0 cm	−2.6%	2.9 cm	7.6%
Test site 2								
Overall	0.2 cm	0.8%	3.4 cm	11.5%	−0.6 cm	−2.3%	2.8 cm	9.9%
DBH ∈ [0, 20) cm	3.7 cm	19.5%	5.6 cm	29.3%	−0.5 cm	−2.2%	2.4 cm	11.3%
DBH ∈ [20, 30) cm	0.6 cm	2.3%	2.5 cm	9.3%	−0.5 cm	−1.7%	2.6 cm	10.1%
DBH ∈ [30, 40) cm	−0.4 cm	−1.2%	4.2 cm	12.5%	−0.9 cm	−2.7%	3.1 cm	9.8%
DBH ∈ [40, ∞) cm	−1.4 cm	−3.3%	3.2 cm	7.6%	−1.5 cm	−3.9%	2.5 cm	6.6%
Test site 3								
Overall	0.9 cm	3.9%	3.5 cm	14.6%	0.8 cm	3.3%	2.9 cm	12.5%
DBH ∈ [0, 20) cm	1.5 cm	9.1%	3.6 cm	20.8%	1.3 cm	7.5%	3.1 cm	18.6%
DBH ∈ [20, 30) cm	0.8 cm	3.5%	3.5 cm	14.4%	0.7 cm	3.1%	2.7 cm	11.4%
DBH ∈ [30, 40) cm	0.2 cm	0.6%	3.0 cm	9.3%	0.0 cm	0.1%	3.4 cm	11.1%
DBH ∈ [40, ∞) cm	−1.3 cm	−3.0%	1.4 cm	3.2%	−1.1 cm	−2.8%	2.0 cm	4.9%

Table A.3
Bias and RMSE of stem volume estimates on the three test sites for the scenario *as many trees as possible*. In addition to the overall bias and RMSE, we also report the bias and RMSE for each of the four DBH categories.

	Stem volume			
	Bias	rbias	RMSE	rRMSE
Test site 1				
Overall	53 dm^3	7.7%	122 dm^3	17.7%
DBH ∈ [0, 20) cm	78 dm^3	32.2%	143 dm^3	58.8%
DBH ∈ [20, 30) cm	42 dm^3	6.9%	100 dm^3	16.3%
DBH ∈ [30, 40) cm	51 dm^3	4.6%	138 dm^3	12.3%
DBH ∈ [40, ∞) cm	99 dm^3	6.0%	178 dm^3	10.7%
Test site 2				
Overall	−49 dm^3	−5.1%	180 dm^3	19.0%
DBH ∈ [0, 20) cm	72 dm^3	16.8%	428 dm^3	100.0%
DBH ∈ [20, 30) cm	−47 dm^3	−6.1%	131 dm^3	17.1%
DBH ∈ [30, 40) cm	−54 dm^3	−4.7%	203 dm^3	17.5%
DBH ∈ [40, ∞) cm	−121 dm^3	−6.7%	210 dm^3	11.6%
Test site 3				
Overall	65 dm^3	12.4%	154 dm^3	29.3%
DBH ∈ [0, 20) cm	77 dm^3	32.8%	142 dm^3	60.4%
DBH ∈ [20, 30) cm	65 dm^3	12.1%	149 dm^3	27.9%
DBH ∈ [30, 40) cm	44 dm^3	4.5%	208 dm^3	21.1%
DBH ∈ [40, ∞) cm	61 dm^3	3.2%	102 dm^3	5.3%

References

Al-Sharadqah, A., Chernov, N., 2009. Error analysis for circle fitting algorithms. Electr. J. Stat. 3, 886–911.

Bienert, A., Scheller, S., Keane, E., Mohan, F., Nugent, C., 2007. Tree detection and diameter estimations by analysis of forest terrestrial laserscanner point clouds. In: ISPRS Workshop On Laser Scanning, 36, pp. 50–55.

Balenović, I., Liang, X., Jurjević, L., Hyyppä, J., Seletković, A., Kukko, A., 2021. Hand-held personal laser scanning–current status and perspectives for forest inventory application. Croat. J. For. Eng.: J. Theory Appl. Forestry Eng. 42 (1), 165–183.

Bienert, A., Georgi, L., Kunz, M., Maas, H.-G., von Oheimb, G., 2018. Comparison and combination of mobile and terrestrial laser scanning for natural forest inventories. Forests 9 (7), 395.

Brede, B., Lau, A., Bartholomeus, H., Kooistra, L., 2017. Comparing RIEGL RiCOPTER UAV LiDAR derived canopy height and DBH with terrestrial LiDAR. Sensors 17 (10), 2371.

Čerňava, J., Mokroš, M., Tuček, J., Antal, M., Slatkovská, Z., 2019. Processing chain for estimation of tree diameter from GNSS-IMU-based mobile laser scanning data. Rem. Sens. 11 (6), 615.

Chen, S., Liu, H., Feng, Z., Shen, C., Chen, P., 2019. Applicability of personal laser scanning in forestry inventory. PLoS One 14 (2), e0211392.

De Boor, C., 1978. A Practical Guide to Splines, vol. 27. springer-Verlag, New York.

Ester, M., Kriegel, H.-P., Sander, J., Xu, X., 1996. A density-based algorithm for discovering clusters in large spatial databases with noise. Kdd 96, 226–231.

EU commission. Climate action - forests and agriculture. https://ec.europa.eu/clima/eu-action/forests-and-agriculture_fi. (Accessed 22 November 2021).

Fischler, M.A., Bolles, R.C., 1981. Random sample consensus: a paradigm for model fitting with applications to image analysis and automated cartography. Commun. ACM 24 (6), 381–395.

Future of the European Forest-Based Sector. Structural Changes towards bioeconomy. https://efi.int/sites/default/files/files/publication-bank/2018/efi_wsctu6_2014.pdf. (Accessed 22 November 2021).

Gollob, C., Ritter, T., Nothdurft, A., 2020. Forest inventory with long range and high-speed personal laser scanning (PLS) and simultaneous localization and mapping (SLAM) technology. Rem. Sens. 12 (9), 1509.

Hackenberg, J., Spiecker, H., Calders, K., Disney, M., Raumonen, P., 2015. SimpleTree—an efficient open source tool to build tree models from TLS clouds. Forests 6 (11), 4245–4294.

Hao, Y., Widagdo, F.R.A., Liu, X., Quan, Y., Dong, L., Li, F., 2021. Individual tree diameter estimation in small-scale forest inventory using UAV laser scanning. Rem. Sens. 13 (1), 24.

Hunčaga, M., Chudá, J., Tomaštík, J., Slámová, M., Koreň, M., Chudý, F., 2020. The comparison of stem curve accuracy determined from point clouds acquired by different terrestrial remote sensing methods. Rem. Sens. 12 (17), 2739.

Hyyppä, E., Muhojoki, J., Yu, X., Kukko, A., Kaartinen, H., Hyyppä, J., 2021a. Efficient coarse registration method using translation-and rotation-invariant local descriptors towards fully automated forest inventory. ISPRS Open J. Photogr. Rem. Sens., 100007

Hyyppä, J., Yu, X., Hakala, T., Kaartinen, H., Kukko, A., Hyyti, H., Muhojoki, J., Hyyppä, E., 2021b. Under-canopy UAV laser scanning providing canopy height and stem volume Accurately. Forests 12 (7).

Hyyppä, E., Yu, X., Kaartinen, H., Hakala, T., Kukko, A., Vastaranta, M., Hyyppä, J., 2020a. Comparison of backpack, handheld, under-canopy UAV, and above-canopy UAV laser scanning for field reference data collection in boreal forests. Rem. Sens. 12 (20), 3327.

Hyyppä, E., Hyyppä, J., Hakala, T., Kukko, A., Wulder, M.A., White, J.C., Pyörälä, J., Yu, X., Wang, Y., Virtanen, J.-P., Pohjavirta, O., Liang, X., Holopainen, M., Kaartinen, H., 2020b. Under-canopy UAV laser scanning for accurate forest field measurements. ISPRS J. Photogrammetry Remote Sens. 164, 41–60.

Hyyppä, J., Inkinen, M., 1999. Detecting and estimating attributes for single trees using laser scanner. Photogramm. J. Finland 16, 27–42.
Hyyppä, E., Kukko, A., Kaijaluoto, R., White, J.C., Wulder, M.A., Pyörälä, J., Liang, X., Yu, X., Wang, Y., Kaartinen, H., Virtanen, J.-P., Hyyppä, J., 2020c. Accurate derivation of stem curve and volume using backpack mobile laser scanning. ISPRS J. Photogrammetry Remote Sens. 161, 246–262.
IUCN. Our work. https://www.iucn.org/theme/forests/our-work. (Accessed 22 November 2021).
Jaakkola, A., Hyyppä, J., Kukko, A., Yu, X., Kaartinen, H., Lehtomäki, M., Lin, Y., 2010. A low-cost multi-sensoral mobile mapping system and its feasibility for tree measurements. ISPRS J. Photogrammetry Remote Sens. 65 (6), 514–522.
Jaakkola, A., Hyyppä, J., Yu, X., Kukko, A., Kaartinen, H., Liang, X., Hyyppä, H., Wang, Y., 2017. Autonomous collection of forest field reference—the outlook and a first step with UAV laser scanning. Rem. Sens. 9 (8), 785.
Kangas, A., Astrup, R., Breidenbach, J., Fridman, J., Gobakken, T., Korhonen, K.T., Maltamo, M., Nilsson, M., Nord-Larsen, T., Næsset, E., Olsson, H., 2018. Remote sensing and forest inventories in nordic countries–roadmap for the future. Scand. J. For. Res. 33 (4), 397–412.
Kuželka, K., Slavík, M., Surovỳ, P., 2020. Very high density point clouds from UAV laser scanning for automatic tree stem detection and direct diameter measurement. Rem. Sens. 12 (8), 1236.
Liang, X., Hyyppä, J., Kukko, A., Kaartinen, H., Jaakkola, A., Yu, X., 2014a. The use of a mobile laser scanning system for mapping large forest plots. Geosci. Rem. Sens. Lett. IEEE 11 (9), 1504–1508.
Liang, X., Kankare, V., Yu, X., Hyyppä, J., Holopainen, M., 2014b. Automated stem curve measurement using terrestrial laser scanning. IEEE Trans. Geosci. Rem. Sens. 52 (3), 1739–1748.
Liang, X., Kankare, V., Hyyppä, J., Wang, Y., Kukko, A., Haggrén, H., Yu, X., Kaartinen, H., Jaakkola, A., Guan, F., Holopainen, M., Vastaranta, M., 2016. Terrestrial laser scanning in forest inventories. ISPRS J. Photogrammetry Remote Sens. 115, 63–77.
Liang, X., Kukko, A., Hyyppä, J., Lehtomäki, M., Pyörälä, J., Yu, X., Kaartinen, H., Jaakkola, A., Wang, Y., 2018. In-situ measurements from mobile platforms: an emerging approach to address the old challenges associated with forest inventories. ISPRS J. Photogrammetry Remote Sens. 143, 97–107.
Liang, X., Wang, Y., Pyörälä, J., Lehtomäki, M., Yu, X., Kaartinen, H., Kukko, A., Honkavaara, E., Issaoui, A.E., Nevalainen, O., Vaaja, M., Virtanen, J.-P., Katoh, M., Deng, S., 2019. Forest in situ observations using unmanned aerial vehicle as an alternative of terrestrial measurements. Forest Ecosystems 6 (1), 20.
Meyer, F., 1994. Topographic distance and watershed lines. Signal Process. 38 (1), 113–125.
Miettinen, M., Kulovesi, J., Kalmari, J., Visala, A., 2010. New measurement concept for forest harvester head. In: Field and Service Robotics. Springer, pp. 35–44.
Næsset, E., Gobakken, T., Holmgren, J., Hyyppä, H., Hyyppä, J., Maltamo, M., Nilsson, M., Olsson, H., Persson, Å., Söderman, U., 2004. Laser scanning of forest resources: the nordic experience. Scand. J. For. Res. 19 (6), 482–499.
Oveland, I., Hauglin, M., Giannetti, F., Schipper Kjørsvik, N., Gobakken, T., 2018. Comparing three different ground based laser scanning methods for tree stem detection. Rem. Sens. 10 (4), 538.
Pollock, D.S.G., 1993. Smoothing with Cubic Splines.
Puliti, S., Breidenbach, J., Astrup, R., 2020. Estimation of forest growing stock volume with UAV laser scanning data: can it be done without field data? Rem. Sens. 12 (8), 1245.
Raumonen, P., Kaasalainen, M., Åkerblom, M., Kaasalainen, S., Kaartinen, H., Vastaranta, M., Holopainen, M., Disney, M., Lewis, P., 2013. Fast automatic precision tree models from terrestrial laser scanner data. Rem. Sens. 5 (2), 491–520.
Shimizu, K., Nishizono, T., Kitahara, F., Fukumoto, K., Saito, H., 2022. Integrating terrestrial laser scanning and unmanned aerial vehicle photogrammetry to estimate individual tree attributes in managed coniferous forests in Japan. Int. J. Appl. Earth Obs. Geoinf. 106, 102658.
Simonse, M., Aschoff, T., Spiecker, H., Thies, M., 2003. Automatic determination of forest inventory parameters using terrestrial laser scanning. In: Proceedings of the Scandlaser Scientific Workshop on Airborne Laser Scanning of Forests, vol. 2003. Citeseer, pp. 252–258.
Tomaštík, J., Saloň, Š., Tunák, D., Chudỳ, F., Kardoš, M., 2017. Tango in forests–an initial experience of the use of the new Google technology in connection with forest inventory tasks. Comput. Electron. Agric. 141, 109–117.
Vandendaele, B., Fournier, R.A., Vepakomma, U., Pelletier, G., Lejeune, P., Martin-Ducup, O., 2021. Estimation of northern hardwood forest inventory attributes using UAV laser scanning (ULS): transferability of laser scanning methods and comparison of automated approaches at the tree-and stand-level. Rem. Sens. 13 (14), 2796.
Wallace, L., Lucieer, A., Watson, C., Turner, D., 2012. Development of a UAV-LiDAR system with application to forest inventory. Rem. Sens. 4 (6), 1519–1543.
Wallace, L., Musk, R., Lucieer, A., 2014. An assessment of the repeatability of automatic forest inventory metrics derived from UAV-borne laser scanning data. IEEE Trans. Geosci. Rem. Sens. 52 (11), 7160–7169.
Wang, Y., Hyyppä, J., Liang, X., Kaartinen, H., Yu, X., Lindberg, E., Holmgren, J., Qin, Y., Mallet, C., Ferraz, A., Torabzadeh, H., Morsdorf, F., Zhu, L., Liu, J., Alho, P., 2016. International benchmarking of the individual tree detection methods for modeling 3-d canopy structure for silviculture and forest ecology using airborne laser scanning. IEEE Trans. Geosci. Rem. Sens. 54 (9), 5011–5027.
Wang, Y., Lehtomäki, M., Liang, X., Pyörälä, J., Kukko, A., Jaakkola, A., Liu, J., Feng, Z., Chen, R., Hyyppä, J., 2019. Is field-measured tree height as reliable as believed–a comparison study of tree height estimates from field measurement, airborne laser scanning and terrestrial laser scanning in a boreal forest. ISPRS J. Photogrammetry Remote Sens. 147, 132–145.
Wieser, M., Mandlburger, G., Hollaus, M., Otepka, J., Glira, P., Pfeifer, N., 2017. A case study of UAS borne laser scanning for measurement of tree stem diameter. Rem. Sens. 9 (11), 1154.
Yu, X., Hyyppä, J., Vastaranta, M., Holopainen, M., Viitala, R., 2011. Predicting individual tree attributes from airborne laser point clouds based on the random forests technique. ISPRS J. Photogrammetry Remote Sens. 66 (1), 28–37.
Zhen, Z., Quackenbush, L.J., Zhang, L., 2016. Trends in automatic individual tree crown detection and delineation—evolution of lidar data. Rem. Sens. 8 (4), 333.